manner as with the Alexa Fluor 488–conjugated phalloidin staining described above. Cell nuclei were then stained with PI. MCECs at the density of 2.0 × 10^5 cells were also seeded, with or without Y-27632, onto Descemet's membrane of four rabbits from each group, and the membrane was then mechanically peeled off at 3 hours after seeding. The adhered MCECs were recovered by trypsin digestion, and the cell numbers were then counted.

Inhibition of ROCK Signaling by siRNA on MCECs in Culture

MCECs seeded at the density of 2.5 × 10^4 cells/cm^2 onto a 24-well plate were incubated with RNAi duplex (ROCK1 Stealth RNAi and ROCK2 Stealth RNAi) and Lipofectamine RNAiMAX according to the manufacturer's protocol. Briefly, 1 day before transfection, the culture medium was replaced with fresh medium without antibiotics. RNAi duplex at the final concentration of 10 nmol/L and Lipofectamine RNAiMAX complexes were added to each well. The MCECs were incubated for 12 hours at 37°C in a CO$_2$ incubator. Random RNAi was used as a control. The MCECs were then seeded at the density of 1.0 × 10^3 cells onto 96-well plates, and the number of attached MCECs was evaluated by use of CellTiter-Glo Luminescent Cell Viability Assay. Knockdown of both ROCK1 and ROCK2, two ROCK isoforms that were identified in the mammalian system,[21] was confirmed by quantitative PCR analysis (data not shown). Representative data were from six independent experiments using three kinds of ROCK1 Stealth RNAi and ROCK2 Stealth RNAi, respectively.

Injection of Cultivated CECs into Monkey Eyes with Corneal Endothelial Dysfunction

To create monkey corneal endothelial pathological dysfunction models, the corneal endothelium of the left eyes of four monkeys was mechanically scraped with a 20-gauge silicone needle under general anesthesia, as described above for the rabbit model. Next, a 2.0 × 10^5 density of cultivated MCECs suspended in 200 μl DMEM supplemented with 100 μmol/L Y-27632 were injected into the anterior chamber of two of the four monkeys. Cultivated MCECs suspended in 200 μl DMEM without Y-27632 were injected into the anterior chamber of the other 2 monkeys. The eyes of all four monkeys were kept in the face-down position for 3 hours under general anesthesia. The MCECs were labeled with DiI before transplantation.[3,4] The corneal appearance of all four monkeys was examined daily by use of a slit-lamp microscope for the first week, and then once per week for the following 3 months. Two monkeys from each group (the MCEC-injection with Y-27632 group, and the MCEC-injection without Y-27632 group) were euthanized at 14 days after the injection, and the other 2 monkeys were euthanized at 3 months after the injection. For flat-mount examinations, whole corneal specimens were fixed in 4% formaldehyde, incubated in 1% BSA to block nonspecific binding, and then prepared for histological examination. To inves-

tigate the phenotype of the reconstructed corneal endothelium, immunohistochemical analyses of actin, ZO-1, and Na$^+$/K$^+$-ATPase were performed in the same manner as that of the above-described rabbit experiments. After the actin immunostaining, the corneal endothelium of the four monkeys was evaluated by KSS-400EB software version 2.71 (Konan Medical, Hyogo, Japan).

Statistical Analysis

The statistical significance (P value) in mean values of the two-sample comparison was determined by Student's t-test. Values shown on the graphs represent the mean ± SEM.

Results

Injection of Cultivated RCECs with ROCK Inhibitor Enables Regeneration of Cornea in Rabbit Corneal Endothelial Dysfunction Model

The third-passaged RCECs exhibited a monolayer of hexagonal shaped cells, similar to in vivo RCECs with a cell density of approximately 2600 cells/mm^2 as previously reported[5,6] (Figure 1A). Cultivated RCECs injected together with Y-27632 were successful in recovering complete transparency of the corneas with pathological dysfunctions. In contrast, RCECs injected without Y-27632 induced hazy and severely edematous corneas, thus indicating that the corneal endothelial dysfunctions were sustained, comparable with those of the control corneas. Slit-lamp microscopy performed at 48 hours after injection revealed complete corneal transparency with the iris and the pupil clearly observed in the eyes injected with RCECs with Y-27632, whereas the iris and pupil could not be observed in the eyes injected with RCECs without Y-27632 and in the control eyes in which the corneal endothelium was mechanically scraped (Figure 1B). Consistent with the slit-lamp microscopy findings, histological analysis performed at 14 days after injection also revealed that the eyes injected with RCECs with Y-27632 had a normal range of corneal thickness, whereas those without Y-27632 exhibited a thick cornea with severe stromal edema. The corneal thicknesses of those specimens were 409 μm and 730 μm, respectively (Figure 1C). In the eyes injected with RCECs with Y-27632, the corneal edema was moderate (<800 μm) at day 1, yet gradually recovered to the normal level. In contrast, in both the control eyes and the eyes injected with RCECs without Y-27632, prominent corneal edema (>1200 μm) was observed at day 1, and corneal edema persisted throughout the observation period (Figure 1D). Next, possible complications associated with cell injection into the anterior chamber were investigated, as the injected cells might possibly interfere with normal aqueous humor outflow and produce an increase in intraocular pressure. No abnormal deposition of the injected DiI-positive RCECs onto the trabecular meshwork or onto the iris and no anatomical abnormality such as mechanical angle closure or peripheral anterior synechia were de-
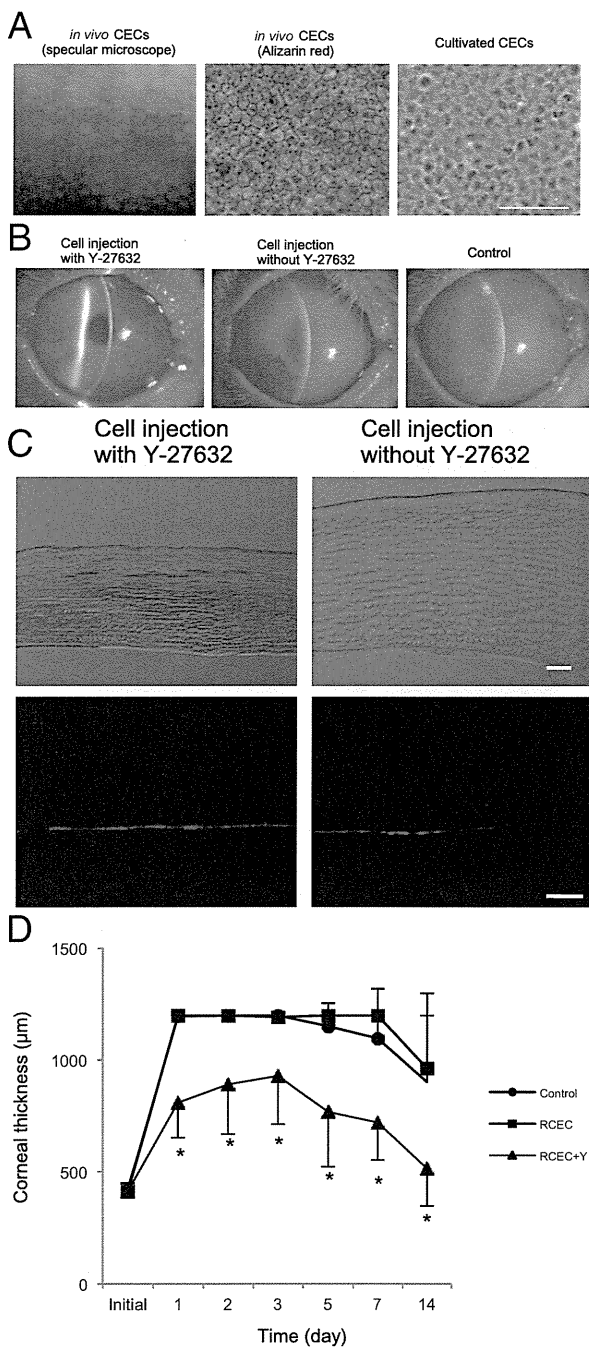
A

in vivo CECs
(specular microscope)

in vivo CECs
(Alizarin red)

Cultivated CECs

B

Cell injection
with Y-27632

Cell injection
without Y-27632

Control

C Cell injection
with Y-27632

Cell injection
without Y-27632

D

Corneal thickness (μm)

- Control
- RCEC
- RCEC+Y

Time (day)

tected (Figure 2A). Intraocular pressures were found to be in the normal range in all groups (Figure 2B). To evaluate the injected CECs proliferation status *in vivo*, a flat-mount cornea was examined at 14 days after injection. Immunofluorescence analysis using the Ki-67 monoclonal antibody (a marker of cell proliferation) revealed that the cell cycle of the nearly all of the injected cells was arrested 2 weeks after injection (Figure 2C). These results
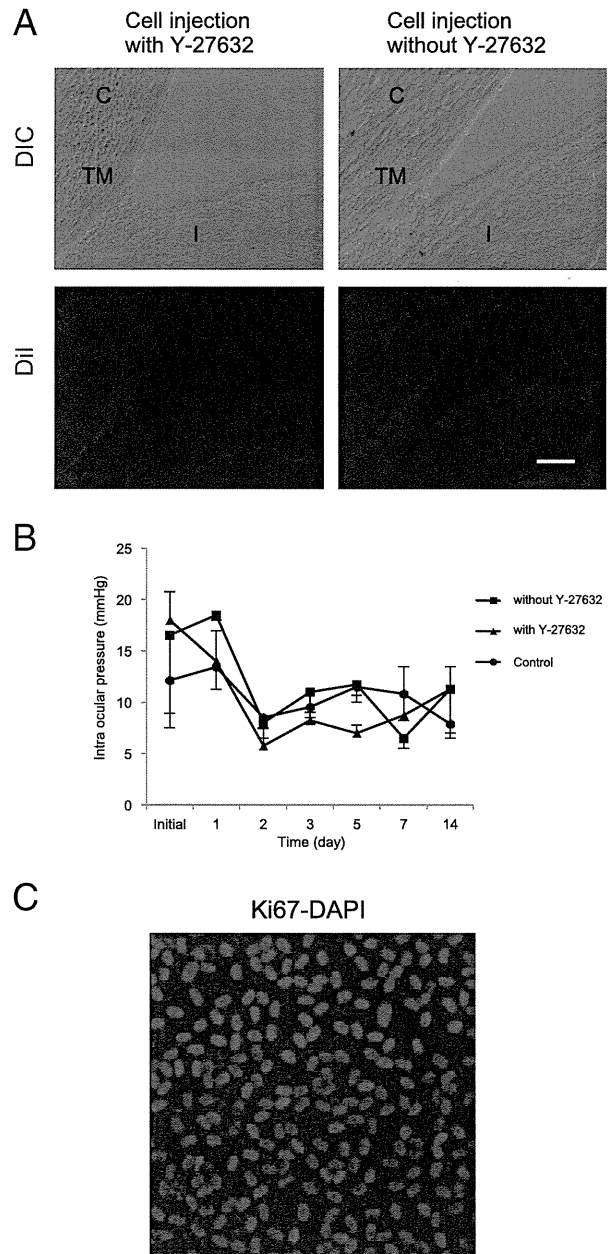
A   Cell injection
with Y-27632

Cell injection
without Y-27632

DIC

DiI

B

Intra ocular pressure (mmHg)

- without Y-27632
- with Y-27632
- Control

Time (day)

C   Ki67-DAPI

Figure 1. Cell regeneration in a rabbit corneal endothelial dysfunction model. **A:** *In vivo* normal corneal endothelium (**left panel:** specular microscope, **middle panel:** Alizarin red staining) and cultivated rabbit corneal endothelial cells (RCECs) (**right panel:** phase contrast image). The cultivated RCECs exhibit a homogeneous monolayer of hexagonal cells with a cell density of approximately 2600 cells/mm^2. The morphology and density of the cultivated RCECs are similar to that of *in vivo* corneal endothelium. Scale bar = 100 μm. **B:** Slit-lamp photographs of rabbit eyes injected with cultivated RCECs with Y-27632, cultivated RCECs without Y-27632, and control corneal endothelial dysfunction model after 48 hours. **C:** Histological analysis of rabbit corneas injected with cultivated RCECs with (**left column**) or without (**right column**) Y-27632 (**top row:** DIC; **bottom row:** DiI). Injection of RCECs with Y-27632 induces a normal-range thickness (409 μm) of the cornea, whereas injection of RCECs without Y-27632 exhibits a thick (730 μm) cornea with severe corneal stromal edema at 14 days after injection. Scale bars: 100 μm. **D:** Time course of corneal thickness measured by ultrasound pachymeter. In control eyes and in the eyes injected with RCECs without Y-27632, the corneal edema is prominent (>1200 μm) at day 1 and persists throughout the observation period. In contrast, in the eyes injected with RCECs with Y-27632, the corneal edema is moderate (<800 μm) at day 1 and gradually recovers to the normal level.

Figure 2. Evaluation of the possible adverse effects of cultivated RCEC injection. **A:** Histological examination of the iris and the angle tissue. **Top row:** representative images of the DIC section taken from the rabbit eye injected with cultivated RCECs with or without Y-27632 after 14 days. **Bottom row:** DiI images of the same sections shown in the **top row.** C, cornea; I, iris; TM, trabecular meshwork. Scale bar = 100 μm. **B:** Intraocular pressures after the injection of RCECs. **C:** Immunohistochemical staining for cell proliferation marker Ki-67 in the reconstructed RCECs in the eye injected with RCECs with Y-27632 on day 14.

indicate that ROCK inhibitor can be safely applied for cell injection therapy.

ROCK Inhibitor Provides RCECs with Phenotype to Reconstruct Corneal Endothelium

At 3 hours after injection, RCECs injected with Y-27632 were found to be markedly adhered to the basement membrane of the corneal endothelium (Figure 3A), suggesting that Y-27632 altered the adhesion properties of the RCECs and up-regulated cell adhesion on the basement membrane in vivo. To ascertain the causal effect of the elevated cell adhesion by Y-27632 in the induction of a pathologically transparent cornea, the histological phenotype of a donor cornea treated with Y-27632 was elucidated using a flat-mount cornea. The expression of ZO-1 and Na^+/K^+-ATPase was evident in RCECs injected with Y-27632, yet it was absent in RCECs injected without Y-27632. RCECs injected with Y-27632 exhibited a monolayer hexagonal cell shape, whereas RCECs injected without Y-27632 exhibited the stratified fibroblastic phenotype. Consistent with the stratified fibroblastic phenotype of RCECs injected without Y-27632, α-SMA (a marker of fibroblastic change) was evident in those RCECs (Figure 3B).

The existence of reconstructed corneal endothelium by the injection of RCECs with Y-27632 that expressed DiI, which labels RCECs, indicated that the injected RCECs contributed to the formation of a monolayer of corneal endothelium and to the inducement of corneal transparency (Figure 3B). However, DiI-expressing cells were also observed in the rabbits injected with RCECs without Y-27632, consistent with the results shown in Figure 1C. The presence of DiI-positive cells in the eyes injected with RCECs without Y-27632 may suggest that a limited number of RCECs were able to adhere to the cornea without the assistance of Y-27632, yet changed their phenotype to that of fibroblastic cells. This finding is consistent with those observed in the clinical setting, in which CECs display a fibroblastic phenotype in cases of corneal endothelial dysfunction.[22,23]

ROCK Inhibitor Y-27632 Enhances Cell Adhesion

To examine the role of the Rho/ROCK signaling pathway in modulating the adhesion properties of primate CECs, cultivated MCECs were plated in combination with ROCK inhibitor Y-27632. Consistent with our previous findings,[20] phase contrast imaging and actin fiber staining revealed elevated cell adhesion in the Y-27632 treated cells (Figure 4A), and the cell adhesion was enhanced at the conventionally used concentration[24] (Figure 4B). MCECs treated with Y-27632 showed a markedly improved expression of vinculin in contrast to the non-treated cells (Figure 4C), suggesting that Y-27632 enhanced the cell adhesion via the induction of focal
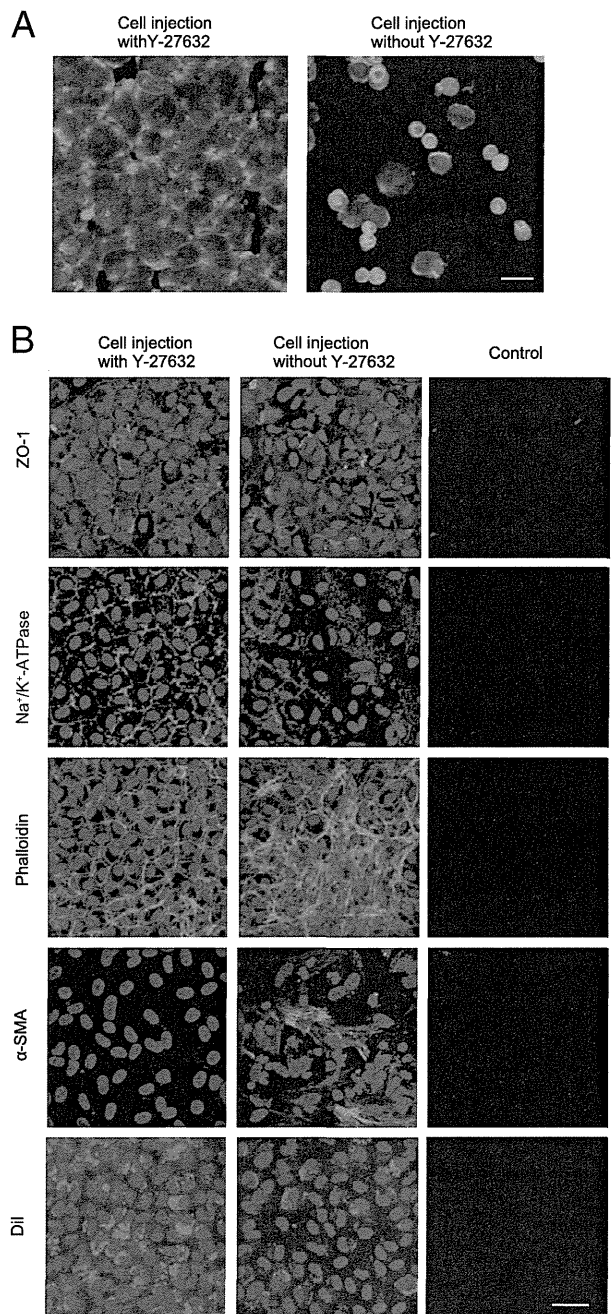

Figure 3. Histological examination of the reconstructed corneal tissue in rabbits after RCEC injection with and without Y-27632. **A:** Flat-mount examination of the posterior side of the corneal tissue 3 hours after RCEC injection. Green fluorescein shows actin-staining (phalloidin), and red shows nuclear staining by propidium iodide (PI). Scale bar = 100 μm. **B:** Histological examination of corneal tissue taken from the rabbit eye 2 weeks after RCEC injection with or without Y-27632. The histological phenotype of the injected RCECs was evaluated by immunofluorescence of ZO-1, Na^+/K^+-ATPase, phalloidin, α-SMA, and DiI after 2 weeks. No cells are observed in the control eyes in which the corneal endothelium was scraped. Scale bar = 100 μm.

adhesion complexes. Considering the interplay between focal adhesion complex molecules and the extracellular matrix,[15] we next attempted to clarify the effect of Y-27632 on MCEC adhesion onto Descemet's membrane (basement membrane). Consistent with the in vivo experiments shown in Figure 3A, an ex vivo culture system
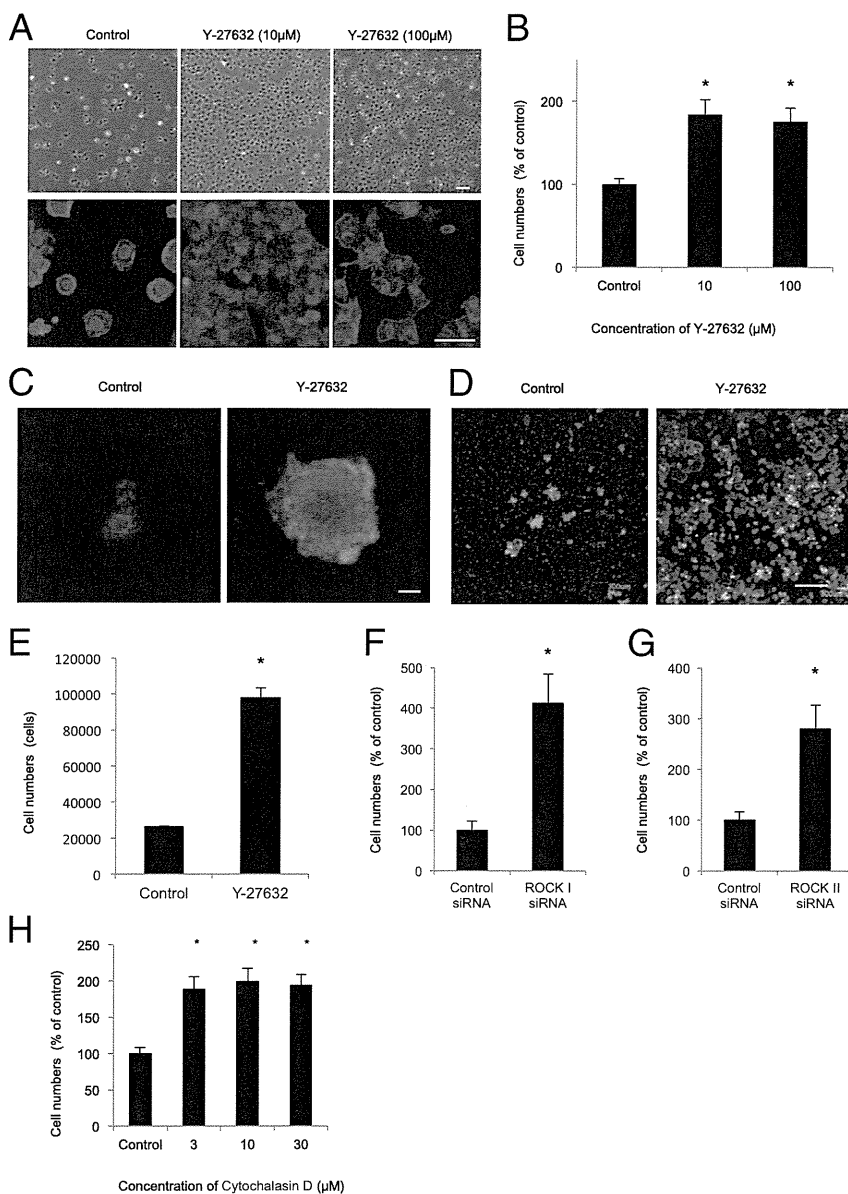
Figure 4. Rho/ROCK signaling pathway modulation of the adhesion properties of primate CECs in culture. **A:** Phase contrast images (**top row**) and actin fiber staining images (**bottom row**) reveal elevated cell adhesion in Y-27632–treated monkey CECs (MCECs) at 24 hours after seeding on a culture dish. Scale bar = 100 μm (**top row**), 50 μm (**bottom row**). **B:** The number of adhered MCECs is significantly enhanced by 10 μmol/L and 100 μmol/L of Y-27632 at 24 hours after seeding. Data are expressed as a percentage of the control, mean ± SEM. *$P <$ 0.01. **C:** Representative immunofluorescence images of MCECs seeded with or without Y-27632 taken after staining with anti-vinculin at 3 hours after seeding. Scale bar = 10 μm. **D:** MCECs were seeded with or without Y-27632 on ex vivo culture system of rabbit Descemet's membrane and stained with actin antibody at 3 hours after seeding. Green fluorescein shows actin staining (phalloidin), and red shows nuclear staining by propidium iodide (PI). Scale bar = 300 μm. **E:** MCECs (density: 2.0 × 10^5 cells) were seeded with or without Y-27632 on rabbit Descemet's membrane, and the number of adhered cells was evaluated at 3 hours after seeding. Data are expressed as mean ± SEM. *$P <$ 0.01. **F** and **G:** Direct contribution of the Rho/ROCK signaling pathway to the regulation of the adhesion properties of CECs was assessed by the knockdown of ROCK1 (**F**) or ROCK2 (**G**). Results are expressed as a percentage of the control, mean ± SEM. *$P <$ 0.01. **H:** MCEC attachment was assessed through the inhibition of actin polymerization by cytochalasin D. Results are expressed as a percentage of the control, mean ± SEM. *$P <$ 0.01.

demonstrated that Y-27632 dramatically enhanced the adhesion of the MCECs onto the basement membrane at 3 hours after seeding (Figure 4, D and E).

The direct contribution of the Rho/ROCK signaling pathway in elevating the adhesion properties was elucidated by the knockdown of ROCK I and ROCK II by RNAi (Figure 4, F and G; confirmed with three independent RNAi). Coincidentally, as with the elevated cell adhesion by Y-27632, the knockdown of both ROCK I and ROCK II strongly enhanced the cell adhesion. Because ROCK signaling is necessary to negatively regulate cell adhesion by inhibiting actin depolymerization, we speculate that inhibition of ROCK by Y-27632 promotes actin reorganization, subsequently inducing the enhancement of cell adhesion. In accordance with that speculation, we found that cytochalasin D, which is additionally capable of inhibiting actin polymerization, also elevated the MCEC adhesion (Figure 4H).

Injection of Cultivated CECs with ROCK Inhibitor Enables Regeneration of Cornea in a Primate Model

The injection of cultivated MCECs combined with Y-27632 was performed in a cynomolgus monkey in which the corneal endothelium was mechanically removed to produce a pathological dysfunction model. To elucidate the long-term efficacy of the injection of CECs with ROCK inhibitor Y-27632, that monkey model was observed for 3 months. In contrast to the rabbit model, slit-lamp microscopy showed that the monkey eyes injected with MCECs, both with and without Y-27632, exhibited complete corneal transparency within 1 week, and that the transparency persisted throughout 3 months of cell injection with a normal range of thickness (<600 μm) (Figure 5A). To evaluate the histological phenotype of donor corneas, two of four mon-
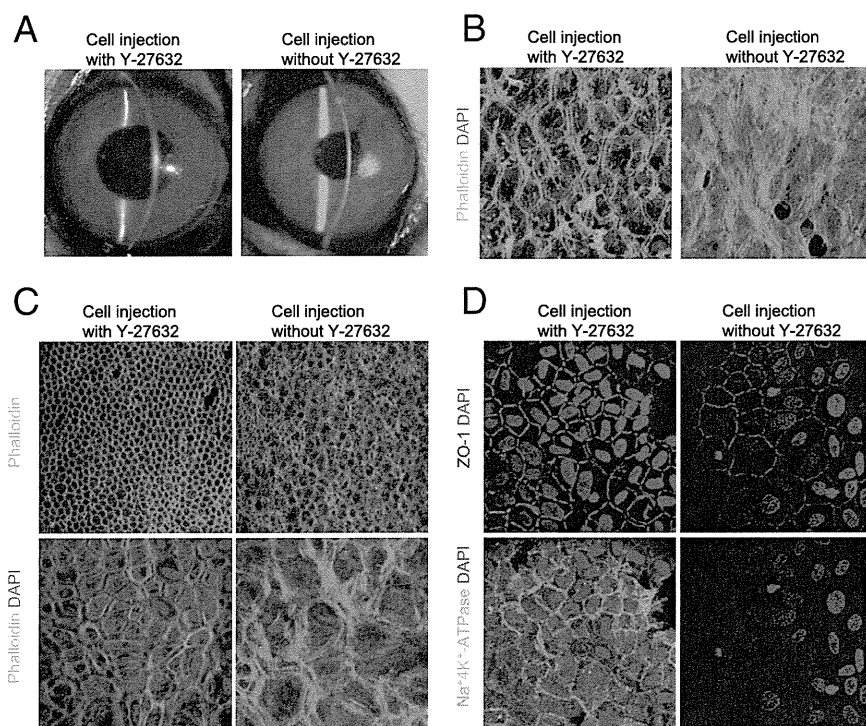
Figure 5. Regeneration of the cornea in a primate model enabled by the injection of cultivated MCECs with Y-27632. **A:** Monkey eyes injected with MCECs with Y-27632 or without Y-27632 exhibit a transparent cornea with a normal range of thickness (<600 μm) after 3 months. **B:** Histological analysis by actin immunostaining after 2 weeks of cell injection of MCECs injected with or without Y-27632. **C:** Histological analysis by actin immunostaining after 3 months of cell injection of MCECs injected with or without Y-27632. **Top row:** lower magnification (green, actin); **bottom row:** higher magnification (green, actin; blue, DAPI). The cell density of the MCECs injected without Y-27632 was 789 cells/mm², whereas that with Y-27632 was 2208 cells/mm². **D:** Histological analysis was performed after immunostaining of ZO-1 (red) or Na⁺/K⁺-ATPase (green). DAPI was used for nuclei staining (blue).

keys were euthanized after 2 weeks of MCEC injection and the other two monkeys after 3 months of MCEC injection (one monkey that received MCEC injection with Y-27632 and one monkey that received MCEC injection without Y-27632, respectively, at each of the two time points). It is notable that the MCECs injected with Y-27632 exhibited a monolayer cell shape, whereas the MCECs injected without Y-27632 exhibited a stratified fibroblastic phenotype at the 2-week time point, which mirrored the rabbit model findings (Figure 5B). Although slit-lamp microscopy showed that the monkey eyes injected with MCECs, both with and without Y-27632, exhibited a transparent cornea with a normal-range corneal thickness, MCECs injected without Y-27632 exhibited a fibroblastic phenotype at the cell density of 789 cells/mm², whereas MCECs injected with Y-27632 exhibited a monolayer hexagonal cell phenotype at the cell density of 2208 cells/mm² (Figure 5C), suggesting that Y-27632 also enhanced the adhesion of MCECs in the *in vivo* monkey model. Consistent with the rabbit experiments, the MCECs injected with Y-27632 expressed ZO-1 and Na⁺/K⁺-ATPase, yet they were expressed to a lesser degree in the MCECs injected without Y-27632 that exhibited the fibroblastic phenotype (Figure 5D).

Discussion

Corneal endothelial dysfunction accompanied by visual disturbance is a major indication for corneal transplantation surgery.[25] Although corneal transplantation is widely performed for corneal endothelial dysfunction, the transplantation of cultivated corneal endothelium is a potential therapeutic strategy. Cultivated CECs derived from older donors have lower proliferative ability, a senescent cell phenotype, and transformed cell morphology, thus suggesting less functional ability than those derived from younger donors.[26] When corneal endothelium is cultured and stocked as "master cells," it allows for the transplantation of CECs derived from younger donors, thus providing cells with high functional ability and an extended longevity. In addition, it enables an HLA-matching transplantation to reduce the risk of rejection[27,28] and to overcome the shortage of donor corneas. In the clinical setting, transplantation of corneal endothelium is technically difficult, because it is a monolayer and is located in the anterior chamber. Thus, that anatomical feature led us to hypothesize that the injection of cultivated CECs would be a potent therapy, even though a previous study reported that cell injection itself was ineffective.[12] The findings of this present study show that the inclusion of ROCK inhibitor Y-27632 elevates the adhesion property of CECs, thus allowing the successful transplantation of CECs to reconstruct functional corneal endothelium damaged by pathological dysfunctions.

We previously reported that the inhibition of ROCK by use of the selective ROCK inhibitor Y-27632 elevates the adhesion of cultured CECs on the substrate, enhances cell proliferation, and suppresses apoptosis.[20] Although the precise underlying mechanisms have yet to be elucidated, those distinct positive effects of ROCK inhibition enable the establishment of the *in vitro* expansion of CECs for cultivated corneal endothelial transplantation.[20] Rho–ROCK signaling carries out a variety of cellular processes such as cell adhesion, morphogenesis, migration, and cell-cycle progression through mediating cytoskeletal dynamics. The Rho GTPase-specific guanine nucleotide exchange factors (Rho GEFs) convert Rho from the guanosine diphosphate (GDP)–bound inactive form to

the guanosine triphosphate (GTP)–bound active form, thus inducing Rho GTPase activity. Rho regulates a variety of cytoskeletal dynamics that underlie cell morphology and adhesion through the activation of ROCK, a major downstream effector.[16,19] ROCK signaling modulates acto-myosin contractility through the regulation of myosin phosphorylation and actin dynamics by promoting nucleation and polymerization or by stimulating the severing and depolymerization of existing actin filaments.[17,29] It is reported that the actin cytoskeleton plays a critical role in regulating the adhesive property through interaction between the actin cytoskeleton and integrin.[14,17,18] Although the adhesive property is dependent on the cell type and the environmental context, ROCK signaling has been shown to negatively regulate the integrin adhesions of monocytes[17] and leukocytes.[18] Findings from a recent study showed that the RhoA–ROCK–PTEN pathway was highly activated when pre-osteoblasts are poorly attached to the substrate, and that the inhibition of this pathway enhances cell adhesion as well as proliferation.[30] Our findings that the inhibition of ROCK signaling by a selective ROCK inhibitor or by the siRNA enhanced adhesive property of CECs are consistent with the findings of those previous studies. Our findings are also supported by our data that inhibiting actin polymerization by cytochalasin D enhances the adhesive property. Furthermore, we found that vinculin, which is involved in the linkage of the integrin adhesion complex to the actin cytoskeleton,[31,32] is upregulated in ROCK-inhibitor-treated CECs. Further investigation is needed to elucidate whether the ROCK inhibitor promotes the focal adhesions through inhibiting actin polymerization and induces the upregulation of cell adhesion properties on the extracellular matrix (ECM).

Corneal endothelial dysfunctions such as Fuchs's endothelial corneal dystrophy, pseudoexfoliation syndrome, keratitis, and injury induce the fibroblastic transformation of CECs.[22,23] In addition, CECs reportedly showed fibroblastic transformation during the wound healing process,[33] and IL-1β–mediated FGF-2 produced after an injury reportedly alters CEC morphology and the actin cytoskeleton in a rabbit freezing injury model.[34] Our findings that RCECs without Y-27632 injected into the anterior chamber of a bullous keratopathy rabbit model exhibited stratified fibroblastic cell morphology and a resultant opaque cornea are consistent with these studies. On the other hand, MCECs without Y-27632 exhibited less fibroblastic phenotype. In our current primate model, a low density of MCECs compensated the pump and barrier functions and resulted in a clear cornea. That finding might possibly be explained by differences in the wound healing process between species.[35,36] However, because CEC density continuously decreases after keratoplasty,[37] reconstructed corneal endothelium with Y-27632 at a high cell density is crucial for the successful long-term outcome of transplantation in the clinical setting. To establish the application of a cultivated CEC injection combined with ROCK inhibitor in clinical settings, transplantation models more akin to humans are required, as rabbit CECs exhibit a high proliferative ability *in vivo*,[38] unlike human CECs. The findings from this present study demonstrated that a monkey eye injected with MCECs with Y-27632 exhibited an almost completely clear cornea. Thus, our primate model–based findings suggest that the cell injection therapy in which the cell adhesion is modulated by ROCK inhibitor might prove to be an effective treatment regimen for human corneal endothelial disorders.

In regard to future clinical applications, ROCK inhibitors have been shown to be useful for a wide range of diseases such as cardiovascular disease, pulmonary disease, cancer, and glaucoma.[21,39–41] Fasudil, one of the ROCK inhibitors, has already been used clinically for the prevention and treatment of cerebral vasospasm, and to date has been therapeutically applied in over 124,000 cases in Japan.[21] Furthermore, we previously demonstrated that a ROCK inhibitor eye drop enhanced corneal endothelial proliferation *in vitro*,[20] as well as in an *in vivo* animal model,[42] and it is currently under clinical research for corneal endothelial dysfunction. These facts suggest that the ROCK inhibitor is a therapeutic tool that can be safely and effectively applied in the clinical setting.

In conclusion, the findings of this present study, which are supported by both rabbit and primate corneal endothelial dysfunction models, indicate that ROCK inhibitor Y-27632 will enable the establishment of a cultivated-CEC–based therapy. Modulating actin cytoskeletal dynamics through Rho-ROCK signaling activity serves as a potential for cell-based regenerative medicine to enhance cell engraftment. This novel strategy of using a cell-based therapy combined with a ROCK inhibitor may ultimately provide clinicians with a new therapeutic modality in regenerative medicine, not only for the treatment of corneal endothelial dysfunctions but also for a variety of pathological diseases.

Acknowledgments

References

1. Gorovoy MS: Descemet-stripping automated endothelial keratoplasty. Cornea 2006, 25:886–889
2. Price FW, Jr., Price MO: Descemet's stripping with endothelial keratoplasty in 50 eyes: a refractive neutral corneal transplant. J Refract Surg 2005, 21:339–345
3. Koizumi N, Sakamoto Y, Okumura N, Okahara N, Tsuchiya H, Torii R, Cooper LJ, Ban Y, Tanioka H, Kinoshita S: Cultivated corneal endothelial cell sheet transplantation in a primate model. Invest Ophthalmol Vis Sci 2007, 48:4519–4526
4. Koizumi N, Sakamoto Y, Okumura N, Tsuchiya H, Torii R, Cooper LJ, Ban Y, Tanioka H, Kinoshita S: Cultivated corneal endothelial transplantation in a primate: possible future clinical application in corneal endothelial regenerative medicine. Cornea 2008, 27 Suppl 1:S48–S55
5. Mimura T, Yamagami S, Yokoo S, Usui T, Tanaka K, Hattori S, Irie S, Miyata K, Araie M, Amano S: Cultured human corneal endothelial cell

transplantation with a collagen sheet in a rabbit model. Invest Ophthalmol Vis Sci 2004, 45:2992–2997

6. Ishino Y, Sano Y, Nakamura T, Connon CJ, Rigby H, Fullwood NJ, Kinoshita S: Amniotic membrane as a carrier for cultivated human corneal endothelial cell transplantation. Invest Ophthalmol Vis Sci 2004, 45:800–806

7. Schachinger V, Erbs S, Elsasser A, Haberbosch W, Hambrecht R, Holschermann H, Yu J, Corti R, Mathey DG, Hamm CW, Suselbeck T, Assmus B, Tonn T, Dimmeler S, Zeiher AM: Intracoronary bone marrow-derived progenitor cells in acute myocardial infarction. N Engl J Med 2006, 355:1210–1221

8. Tateishi-Yuyama E, Matsubara H, Murohara T, Ikeda U, Shintani S, Masaki H, Amano K, Kishimoto Y, Yoshimoto K, Akashi H, Shimada K, Iwasaka T, Imaizumi T: Therapeutic angiogenesis for patients with limb ischaemia by autologous transplantation of bone-marrow cells: a pilot study and a randomised controlled trial. Lancet 2002, 360:427–435

9. Shapiro AM, Lakey JR, Ryan EA, Korbutt GS, Toth E, Warnock GL, Kneteman NM, Rajotte RV: Islet transplantation in seven patients with type 1 diabetes mellitus using a glucocorticoid-free immunosuppressive regimen. N Engl J Med 2000, 343:230–238

10. Yanaga H, Koga M, Imai K, Yanaga K: Clinical application of biotechnically cultured autologous chondrocytes as novel graft material for nasal augmentation. Aesthetic Plast Surg 2004, 28:212–221

11. Mimura T, Shimomura N, Usui T, Noda Y, Kaji Y, Yamgami S, Amano S, Miyata K, Araie M: Magnetic attraction of iron-endocytosed corneal endothelial cells to Descemet's membrane. Exp Eye Res 2003, 76: 745–751

12. Mimura T, Yamagami S, Usui T, Ishii Y, Ono K, Yokoo S, Funatsu H, Araie M, Amano S: Long-term outcome of iron-endocytosing cultured corneal endothelial cell transplantation with magnetic attraction. Exp Eye Res 2005, 80:149–157

13. Patel SV, Bachman LA, Hann CR, Bahler CK, Fautsch MP: Human corneal endothelial cell transplantation in a human ex vivo model. Invest Ophthalmol Vis Sci 2009, 50:2123–2131

14. Sastry SK, Burridge K: Focal adhesions: a nexus for intracellular signaling and cytoskeletal dynamics. Exp Cell Res 2000, 261:25–36

15. Critchley DR: Focal adhesions—the cytoskeletal connection. Curr Opin Cell Biol 2000, 12:133–139

16. Hall A: Rho GTPases and the actin cytoskeleton. Science 1998, 279:509–514

17. Worthylake RA, Lemoine S, Watson JM, Burridge K: RhoA is required for monocyte tail retraction during transendothelial migration. J Cell Biol 2001, 154:147–160

18. Worthylake RA, Burridge K: RhoA and ROCK promote migration by limiting membrane protrusions. J Biol Chem 2003, 278:13578–13584

19. Narumiya S, Tanji M, Ishizaki T: Rho signaling, ROCK and mDia1, in transformation, metastasis and invasion. Cancer Metastasis Rev 2009, 28:65–76

20. Okumura N, Ueno M, Koizumi N, Sakamoto Y, Hirata K, Hamuro J, Kinoshita S: Enhancement on primate corneal endothelial cell survival in vitro by a ROCK inhibitor. Invest Ophthalmol Vis Sci 2009, 50: 3680–3687

21. Liao JK, Seto M, Noma K: Rho kinase (ROCK) inhibitors. J Cardiovasc Pharmacol 2007, 50:17–24

22. Naumann GO, Schlotzer-Schrehardt U: Keratopathy in pseudoexfoliation syndrome as a cause of corneal endothelial decompensation: a clinicopathologic study. Ophthalmology 2000, 107:1111–1124

23. Kawaguchi R, Saika S, Wakayama M, Ooshima A, Ohnishi Y, Yabe H: Extracellular matrix components in a case of retrocorneal membrane associated with syphilitic interstitial keratitis. Cornea 2001, 20:100–103

24. Narumiya S, Ishizaki T, Uehata M: Use and properties of ROCK-specific inhibitor Y-27632. Methods Enzymol 2000, 325:273–284

25. Darlington JK, Adrean SD, Schwab IR: Trends of penetrating keratoplasty in the United States from 1980 to 2004. Ophthalmology 2006, 113:2171–2175

26. Joyce NC, Zhu CC: Human corneal endothelial cell proliferation: potential for use in regenerative medicine. Cornea 2004, 23:S8–S19

27. Khaireddin R, Wachtlin J, Hopfenmuller W, Hoffmann F: HLA-A. HLA-B and HLA-DR matching reduces the rate of corneal allograft rejection. Graefes Arch Clin Exp Ophthalmol 2003, 241:1020–1028

28. Coster DJ, Williams KA: The impact of corneal allograft rejection on the long-term outcome of corneal transplantation. Am J Ophthalmol 2005, 140:1112–1122

29. Ishizaki T, Uehata M, Tamechika I, Keel J, Nonomura K, Maekawa M, Narumiya S: Pharmacological properties of Y-27632, a specific inhibitor of rho-associated kinases. Mol Pharmacol 2000, 57:976–983

30. Yang S, Kim HM: The RhoA-ROCK-PTEN pathway as a molecular switch for anchorage dependent cell behavior. Biomaterials 2012, 33:2902–2915

31. Geiger B: A 130K protein from chicken gizzard: its localization at the termini of microfilament bundles in cultured chicken cells. Cell 1979, 18:193–205

32. Burridge K, Feramisco JR: Microinjection and localization of a 130K protein in living fibroblasts: a relationship to actin and fibronectin. Cell 1980, 19:587–595

33. Ichijima H, Petroll WM, Jester JV, Barry PA, Andrews PM, Dai M, Cavanagh HD: In vivo confocal microscopic studies of endothelial wound healing in rabbit cornea. Cornea 1993, 12:369–378

34. Lee HT, Lee JG, Na M, Kay EP: FGF-2 induced by interleukin-1 beta through the action of phosphatidylinositol 3-kinase mediates endothelial mesenchymal transformation in corneal endothelial cells. J Biol Chem 2004, 279:32325–32332

35. Matsubara M, Tanishima T: Wound-healing of the corneal endothelium in the monkey: a morphometric study. Jpn J Ophthalmol 1982, 26:264–273

36. Matsubara M, Tanishima T: Wound-healing of corneal endothelium in monkey: an autoradiographic study. Jpn J Ophthalmol 1983, 27:444–450

37. Bourne WM, Nelson LR, Hodge DO: Central corneal endothelial cell changes over a ten-year period. Invest Ophthalmol Vis Sci 1997, 38:779–782

38. Van Horn DL, Sendele DD, Seideman S, Buco PJ: Regenerative capacity of the corneal endothelium in rabbit and cat. Invest Ophthalmol Vis Sci 1977, 16:597–613

39. Koga T, Awai M, Tsutsui J, Yue BY, Tanihara H: Rho-associated protein kinase inhibitor, Y-27632, induces alterations in adhesion, contraction and motility in cultured human trabecular meshwork cells. Exp Eye Res 2006, 82:362–370

40. Olson MF: Applications for ROCK kinase inhibition. Curr Opin Cell Biol 2008, 20:242–248

41. Tokushige H, Inatani M, Nemoto S, Sakaki H, Katayama K, Uehata M, Tanihara H: Effects of topical administration of y-39983, a selective rho-associated protein kinase inhibitor, on ocular tissues in rabbits and monkeys. Invest Ophthalmol Vis Sci 2007, 48:3216–3222

42. Okumura N, Koizumi N, Ueno M, Sakamoto Y, Takahashi H, Hirata K, Torii R, Hamuro J, Kinoshita S: Enhancement of corneal endothelium wound healing by Rho-associated kinase (ROCK) inhibitor eye drops. Br J Ophthalmol 2011, 95:1006–1009

A Study of Host Corneal Endothelial Cells After Non-Descemet Stripping Automated Endothelial Keratoplasty

Hiroki Hatanaka, MD,* Noriko Koizumi, MD, PhD,† Naoki Okumura, MD, PhD,*†
Hiroaki Takahashi, MS,† Hidetoshi Tanioka, PhD,* Robert D. Young, PhD,‡
Frances E. Jones, BSc,‡ Andrew J. Quantock, PhD,‡ and Shigeru Kinoshita, MD, PhD*

Purpose: To determine the short-term fate of the host endothelium and Descemet membrane after non-Descemet stripping automated endothelial keratoplasty (nDSAEK).

Methods: Eight unilateral DSAEK (n = 4) or nDSAEK (n = 4) surgeries were performed in the right eyes of 8 rabbits. Corneal transparency and thickness were followed-up by slit-lamp microscopy, and 2 weeks postoperatively, corneas were evaluated by immunohistochemistry and transmission electron microscopy.

Results: Corneas remained clear after both DSAEK and nDSAEK. One week after DSAEK, the stroma-to-stroma surgical interface was identifiable as a zone of fibrotic tissue a few microns thick, whereas in the nDSAEK group, the recipient corneal endothelium and Descemet membrane were clearly visible at the graft–host interface. The retained endothelial cells were positive for Na$^+$/K$^+$-ATPase but assumed a markedly different morphology from healthy endothelial cells, with cell processes extending into the graft stroma or engulfing strands of irregularly dissected grafted stromal tissue where they occasionally appeared to compartmentalize the transplanted matrix and became detached from the underlying Descemet membrane.

Conclusions: Host endothelial cells 2 weeks after nDSAEK express markers of pump function, but appear to be morphologically altered, occasionally detaching from the adjacent Descemet membrane, extending into the graft stroma or engulfing strands of the grafted stroma at the interface. The short-term persistence and subsequent phenotypical alternation of residual endothelial cells, aligned to structural changes to Descemet membrane, might influence graft adherence after nDSAEK.

Corneal endothelial disorders such as Fuchs endothelial dystrophy or pseudophakic bullous keratopathy lead to irreversible corneal endothelial dysfunction. Penetrating keratoplasty has been widely performed for the restoration of endothelial function. However, this has several potential adverse effects such as the occurrence of irregular astigmatism, suture-induced problems, and fragility against trauma. Alternative methods for replacing the endothelium have been developed lately and include posterior lamellar keratoplasty, deep lamellar endothelial keratoplasty, Descemet stripping endothelial keratoplasty, Descemet stripping automated endothelial keratoplasty (DSAEK), and Descemet membrane endothelial keratoplasty.[1–4]

Recently, a new modified form of DSAEK has been reported, which has been termed non-Descemet stripping automated endothelial keratoplasty (nDSAEK).[5] This procedure differs from DSAEK in that the host Descemet membrane and endothelium are not surgically removed before the introduction of the posterior lamellar graft. nDSAEK has been shown to be efficient for the treatment of endothelial dysfunction not associated with guttata, with rapid visual recovery and minimal induced astigmatism.[5] In contrast, donor dislocation has been reported after nDSAEK,[5] and subclinical corneal abnormalities have been observed by laser confocal microscopy.[6] We hypothesize that the continued presence of the host endothelium and Descemet membrane may adversely affect the adherence of the posterior graft tissue. The aim of this study was to understand more fully the change of function and anatomy of the residual endothelial cells in the immediate post-nDSAEK period in a rabbit model.

MATERIALS AND METHODS

Surgical Procedure

Japanese white rabbits (female, 9–10 weeks old, 2–3 kg body weight; Shimizu Laboratory Supplies Co, Ltd, Kyoto, Japan) were used as an animal model for corneal endothelial

transplantation and treated in accordance with the Association for Research in Vision and Ophthalmology Statement for the Use of Animals in Ophthalmic and Vision Research. The experimental procedures were approved by the Animal Care and Use Committee of Kyoto Prefectural University of Medicine (Approval No. 12-12).

Eight corneas of 4 rabbits, euthanized by injection with pentobarbital sodium (130 mg/kg; Kyoritsu, Tokyo, Japan), were used as donor material, with preparation of donor lenticules immediately preceding the DSAEK or nDSAEK procedures. First, a donor corneoscleral button was placed on a Barron artificial anterior chamber (Katena Products, Denville, NJ), after which saline was infused into the chamber. For each button, a corneal endothelial graft, 100 to 200 μm thick and 8 mm in diameter, was dissected manually using a DALK spatula set (Dutch Ophthalmic Research Center, Zuidland, the Netherlands) and separated by dermal punch using the technique described by Melles et al.[7] These 8 graft tissues were then implanted unilaterally into the right eyes of 8 rabbits as described in the following, 4 using the DSAEK technique and 4 using nDSAEK.

One week before the DSAEK and nDSAEK surgeries, lensectomies and peripheral iridectomies were performed in the right eyes of the 8 rabbits. At surgery, recipient rabbits were anesthetized by intramuscular injection of a mixture of ketamine hydrochloride (70.4 mg/kg; Sankyo, Tokyo, Japan), xylazine (11.8 mg/kg; Bayer, Munich, Germany), and topical oxybuprocaine. Pupils were expanded with topical tropicamide. Surgery was performed on the right eye of each rabbit using the modified technique described by Price et al.[3] First, for DSAEK, a 3-mm limbal-corneal incision was made and the endothelium/Descemet membrane was mechanically scraped using a modified Price-Sinskey hook (ASICO, Westmont, IL) while infusing air into the anterior chamber through a 25-gauge cannula. The scraped area measured at least 9 mm in diameter, and the denuded area was confirmed by 0.04% trypan blue staining during surgery. Descemet membrane scraping was not done in the nDSAEK group. Next, a Busin glide (Moria, Doylestown, PA) was loaded with the donor tissue, oriented so that its endothelial side faced the anterior chamber. This was coated with Viscoat (Alcon, Fort Worth, TX) to protect the cells from physical damage. The graft was pulled into the Busin glide opening, and a 25-gauge anterior capsular forceps (Inami, Tokyo, Japan) that entered the opposite side of the anterior chamber through a small incision was used to grasp the graft. The inserted graft was then attached to the recipient cornea by air injection, and the incision was closed with 10-0 nylon sutures. After surgery, all animals received 0.3% ofloxacin ointment and were maintained with the right side of the face facing downward for 30 to 60 minutes. At days 1, 3, 5, 7, and 14 after surgery, corneal transparency was assessed by the use of a slit-lamp microscope.

Immunohistochemistry

Two weeks after surgery, animals were killed by injection with pentobarbital sodium (130 mg/kg; Kyoritsu),

and 4% paraformaldehyde was perfused into the anterior chamber and applied dropwise to the ocular surface for 5 to 10 minutes. Corneoscleral buttons were then excised and immersed in 20% sucrose overnight at 4°C and embedded in optimal cutting temperature compound at −80°C. Sections (10 μm thick) were cut, fixed in 4% formaldehyde for 5 minutes at room temperature, permeabilized for 5 minutes in phosphate-buffered saline (PBS) containing 0.5% Triton X-100, washed, and incubated for 60 minutes with 1% bovine serum albumin. This was followed by overnight incubation at 4°C with 1:100 diluted mouse anti-Na$^+$/K$^+$-ATPase antibody (Anti-Na+/K+ ATPase α-1, clone C464-6; Millipore, Billerica, MA) and 3 washes in PBS. Sections were then incubated at room temperature with 1:2000 diluted Alexa Fluor 488–conjugated goat antimouse IgG (Invitrogen Corporation) and washed 3 times. They were subsequently washed with PBS in the dark, mounted on glass slides with antifading mounting medium containing 4′,6-diamidino-2-phenylindole (DAPI) (VECTASHIELD; Vector Laboratories, Burlingame, CA) and inspected with a fluorescence microscope (Olympus, Tokyo, Japan).

Transmission Electron Microscopy

For light and transmission electron microscopy, excised corneas, which had first been perfused in situ for 5 to 10 minutes with 4% paraformaldehyde as was done for the immunohistochemistry preparation, were fixed in 2.5% glutaraldehyde and 2% paraformaldehyde in 0.1 M Sorensen buffer, pH 7.2 to 7.4, for 2 to 3 hours at room temperature. After several washes in the buffer and postfixation with 1% osmium tetroxide, they were dehydrated and embedded in Araldite resin. Semithin sections (1 μm thick) were stained with toluidine blue for inspection at the light microscope level, whereas ultrathin sections (~90 nm thick) were collected on uncoated copper grids for study by transmission electron microscopy. Contrasting of ultrathin sections was with phosphotungstic acid and aqueous uranyl acetate (1 and 12 minutes, respectively), followed by Reynolds lead citrate (5 minutes) with washes in between. Stained sections were examined in a JEOL 1010 transmission electron microscope (JEOL, Tokyo, Japan), equipped with a Gatan ORIUS SC1000 CCD camera.

RESULTS

Slit-Lamp Microscopy

Slit-lamp examinations of the 8 operated eyes revealed that the corneas were clear in both the nDSAEK and the DSAEK groups at postoperative day 7 (Fig. 1). In the nDSAEK group, 1 lamellar graft had become dislocated the day after surgery, but it readhered to the center of the cornea after the injection of air into the anterior chamber. Slit-lamp examination revealed that graft adhesion was good in both groups. However, after nDSAEK, folds appeared and became progressively more noticeable in number and size at the graft edge in all 4 cases (Fig. 2).
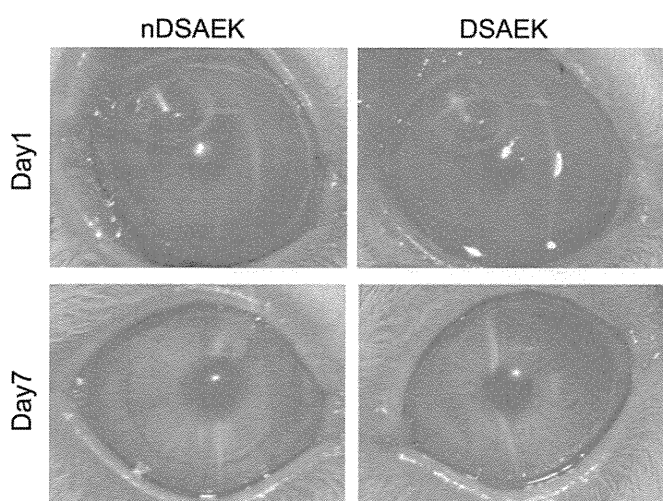
- 146 -

nDSAEK   DSAEK   nDSAEK   DSAEK

FIGURE 1. Slit-lamp photographs 1 and 7 days after surgery, indicating cloudiness at 1 day with a return to clarity by 7 days after both DSAEK and nDSAEK.

Immunohistochemistry

Histological sections of corneas healing after DSAEK indicated a well-adhered graft with a thin and fairly indistinct stroma-to-stroma interface (Fig. 3). Histology of post-nDSAEK tissue, in contrast, showed the clear retention of residual Descemet membrane and endothelium at the surgical interface, sandwiched between host stroma and graft stroma (Fig. 3). The recipient corneal endothelial cells retained in the cornea after nDSAEK were also identified on histochemistry by the nuclear stain, DAPI, which revealed a line of positive cells at the junction between the host and graft tissues 14 days after surgery (Fig. 4). Immunohistochemistry, moreover, suggested that the sandwiched host endothelial cells retained a lot of cellular function because they were positive for Na^+/K^+-ATPase protein (Fig. 4).

Transmission Electron Microscopy

The lamellar graft in nDSAEK adhered well to the residual endothelium/Descemet layer; nevertheless, at the
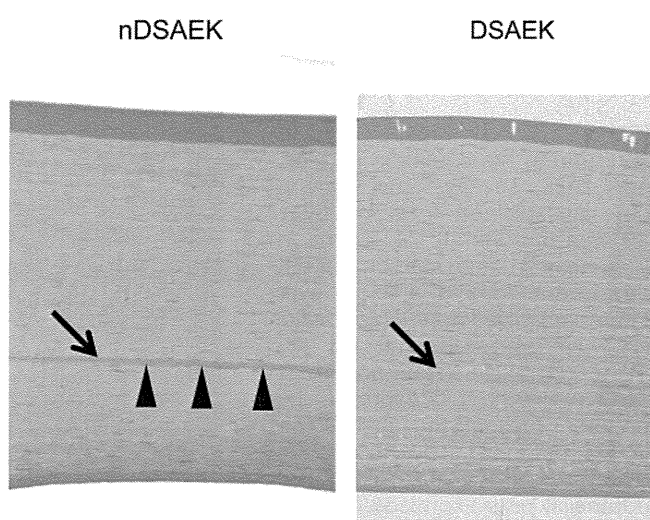
FIGURE 3. Light micrographs of DSAEK and nDSAEK corneas 7 days after surgery taken from semithin sections of resin-embedded tissue stained with 1% toluidine blue. The graft–host interface is indicated by an arrow, with the host Descemet membrane and endothelium clearly visible in nDSAEK sections (arrowheads). Bar = 50 μm.

electron microscopic level, distinct phenotypic and morphological changes in the endothelial cells and Descemet membrane were evident (Fig. 5A, B). Notably, the endothelial cells often appeared to extend cell processes into the adjacent grafted stroma, resulting in partial compartmentalization of the matrix, or to engulf loose strands on the irregular surface of grafted stroma, which might include some phagocytic activity (Figs. 5A, B). Duplication of Descemet membrane was also seen, with the membrane present at the apical and basal sides of the host endothelium (Fig. 6A). Residual endothelial cells also sometimes became detached from the host Descemet membrane, with a layer of stromal tissue that resembled fibrotic tissue lying between the cells and Descemet membrane (Fig. 6B). In these areas of graft–host interface, portions of duplicated, or split and invaded, Descemet membrane could also often be seen in close association with the detached host endothelium (Fig. 6B).

DISCUSSION

nDSAEK is a contemporary modification of the gamut of endothelial keratoplasties, and although clinical outcomes are promising, there is a dearth of fundamental knowledge about the postoperative fate of the residual endothelium and Descemet membrane. This knowledge is important because it is suspected that the good adherence of the graft interface after DSAEK—where the host endothelium and Descemet membrane are removed—is, much like after laser in situ keratomileusis, a result of direct stroma-to-stroma contact, and we hypothesize that the retained endothelial cells and Descemet membrane might have some effect on this adhesion.

Our investigations reveal that, 2 weeks after nDSAEK, endothelial cells persist at the boundary between host and graft and also express Na^+/K^+-ATPase protein. Often, these
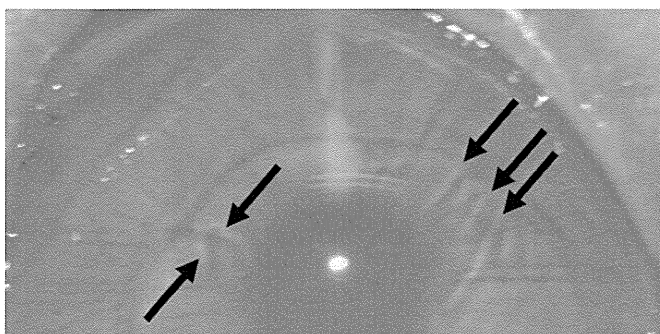

FIGURE 2. A slit-lamp photograph of a representative cornea in the nDSAEK group, 7 days after surgery. The folds seen at the edge of the graft (arrows) are typical of all 4 nDSAEK surgeries and increased in number and size throughout the observation period.

- 147 -

FIGURE 4. Function-related protein expression in the cornea in nDSAEK and DSAEK, 14 days after surgery. Some unexplained focal positivity was seen throughout the stroma in all corneas studied, and in DSAEK and nDSAEK corneas, a single layer of immunolabeled donor endothelial cells were observed with Na$^+$/K$^+$-ATPase (arrows). The graft–host interface was not identifiable by immunohistochemistry in DSAEK corneas, but in nDSAEK corneas, the retained monolayer of host corneal endothelial cells expressed Na$^+$/K$^+$-ATPase. These were also stained with the nuclear stain, DAPI, which formed a discontinuous line at the graft–host interface (arrowheads). Bar = 100 μm.
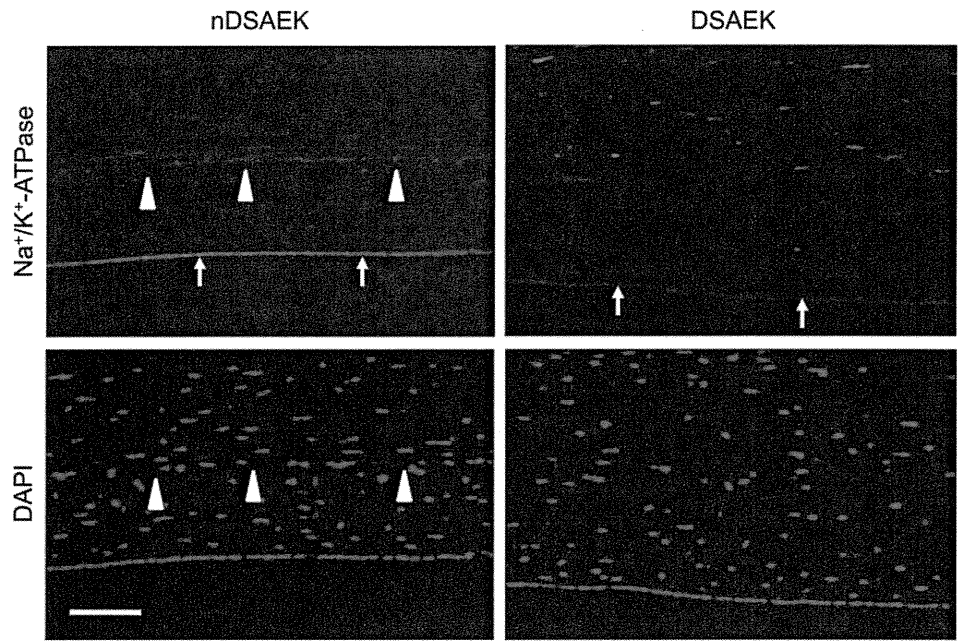
cells are closely apposed to the residual host Descemet membrane and form a monolayer not unlike that in a healthy endothelium. On occasion, however, the endothelial cells assume an abnormal phenotype, with cell processes extending into the graft stroma or engulfing loose strands of the dissected stromal matrix. Deposition of fibrotic tissue between the host endothelium and residual Descemet membrane was also found, and we speculate that phenotypic changes in the host endothelium represent the early stages of cellular transformation under stress[8,9] or some phagocytic activity of the endothelial cells. In the normal adult cornea, the endothelium lays down collagen type IV at its distal surface, which constitutes the posterior nonbanded portion of Descemet membrane. It might be the case that the endothelium deposits collagen type IV at its proximal surface also, only for this to be removed by the fluid dynamics of the aqueous humor. If this is so, it might explain the presence of duplicated basement membrane–like material adjacent to the proximal side of the host endothelium.

Immunohistochemistry indicates that retained endothelial cells 2 weeks after nDSAEK display a partial endothelial phenotype as evidenced by Na$^+$/K$^+$-ATPase protein expression. This leads us to consider the potential metabolic response of the sandwiched endothelial cells and the likelihood of any pump function. The corneal stroma will swell rapidly if bathed in an aqueous medium,[10] a phenomenon that
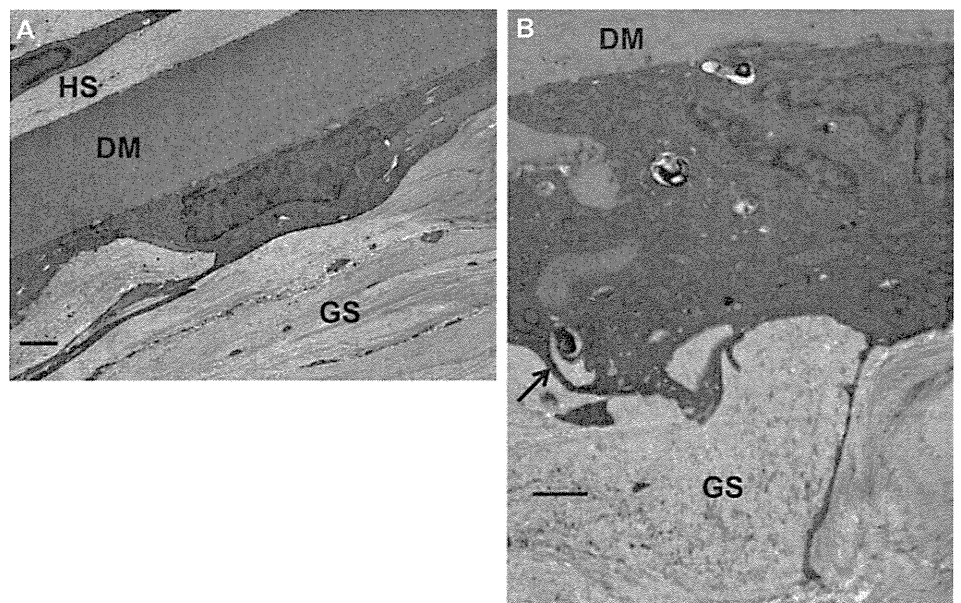

FIGURE 5. A, An electron micrograph of residual host Descemet membrane (DM) and a well-adhered endothelium after nDSAEK. Bar = 2.5 μm. B, An electron micrograph of residual host DM and endothelium (arrow) after nDSAEK. Bar = 500 nm. Endothelial cells appear to extend into graft stroma or engulf loose connective tissue strands on the surface of the transplanted tissue. GS, graft stroma; HS, host stroma.

FIGURE 6. A, An electron micrograph of residual host Descemet membrane (DM) and a well-adhered endothelium (arrow) sandwiched between host stroma (HS) and graft stroma (GS) after nDSAEK. Bar = 2 μm. B, An electron micrograph of residual host DM and endothelium sandwiched between HS and GS after nDSAEK. The endothelium (arrow) has become detached from DM, and a fibrotic stromal matrix (indicated by an asterisk) exists between the endothelium and DM. Bar = 2 μm.
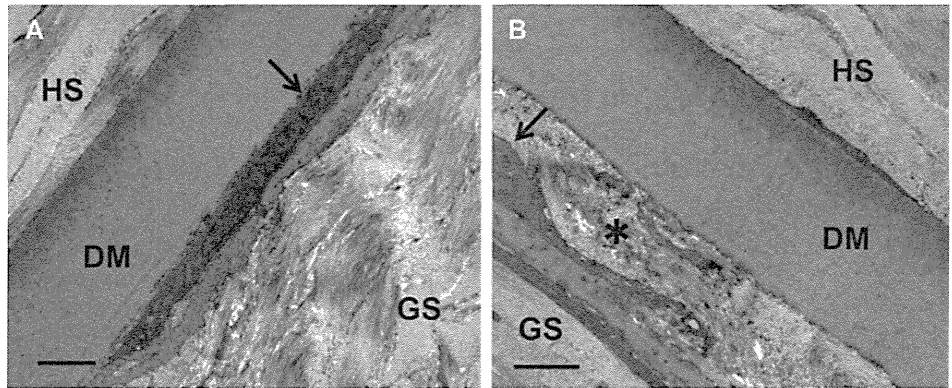
is due predominantly to the presence of collagen-bound sulfated proteoglycans[11] and chloride anions that are electrostatically associated with the matrix in a transient manner.[12,13] This swelling tendency is neutralized in the physiologically normal cornea by the continuous removal of bicarbonate ions from the corneal stroma by the metabolically active endothelial pump.[14] The presence of a monolayer of residual host endothelial cells after nDSAEK, aligned with immunohistochemical evidence of Na^+/K^+-ATPase protein expression, prompts us to consider the likelihood of a dual bicarbonate pump in these corneas, with functionality in both the new grafted endothelium and the trapped host endothelium. Physiological reasoning and a consideration of most of the key aspects of endothelial metabolism indicate no reason why the sandwiched endothelium in the early stages after nDSAEK could not function as an active bicarbonate pump. However, we are reminded of a series of experiments (S. A. Hodson, PhD, personal communication, August 2011), which indicated that endothelial pump function examined in vitro was stopped when the circulation of fluid bathing the apical face of the endothelium was temporarily ceased, only to start up again once fluid circulation was resumed. This was attributed to the nonremoval and consequent build up of lactic acid near the endothelium, something that would likely occur in the graft stroma adjacent to the residual endothelium in nDSAEK. Based on this reasoning, aligned to the longer term morphological changes and transformation of the trapped endothelial cells in nDSAEK, we suspect little if any functionality in the retained host endothelium.

nDSAEK is a useful surgery that can lead to favorable clinical outcomes, as has been reported by other investigators. It appears that in the early postoperative period, in rabbits at least, healing is accompanied by the close apposition between graft stroma and the apical surface of host endothelial cells that retain some pump function. We also note that the series of phenomena reported here may not be restricted to nDSAEK but might occur in DSAEK too at the corneal periphery if the lateral extent of the graft material overlaps a smaller debrided area.

REFERENCES

1. Melles GR, Lander F, Rietveld FJ. Transplantation of Descemet's membrane carrying viable endothelium through a small scleral incision. *Cornea.* 2002;21:415–418.
2. Terry MA, Ousley PJ. Deep lamellar endothelial keratoplasty in the first United States patients: early clinical results. *Cornea.* 2001;20: 239–243.
3. Price FW Jr, Price MO. Descemet's stripping with endothelial keratoplasty in 50 eyes: a refractive neutral corneal transplant. *J Refract Surg.* 2005;21:339–345.
4. Melles GRJ, Ong TS, Ververs B, et al. Descemet membrane endothelial keratoplasty (DMEK). *Cornea.* 2006;25:987–990.
5. Kobayashi A, Yokogawa H, Sugiyama K. Non-Descemet stripping automated endothelial keratoplasty for endothelial dysfunction secondary to argon laser iridotomy. *Am J Ophthalmol.* 2008;146: 543–549.
6. Kobayashi A, Yokogawa H, Sugiyama K. In vivo laser confocal microscopy after non-Descemet's stripping automated endothelial keratoplasty. *Ophthalmology.* 2009;116:1306–1313.
7. Melles GR, Eggink FA, Lander F, et al. A surgical technique for posterior lamellar keratoplasty. *Cornea.* 1998;17:618–626.
8. Naumann GO, Schlotzer-Schrehardt U. Keratopathy in pseudoexfoliation syndrome as a cause of corneal endothelial decompensation: a clinicopathologic study. *Ophthalmology.* 2000;107:1111–1124.
9. Kawaguchi R, Saika S, Wakayama M, et al. Extracellular matrix components in a case of retrocorneal membrane associated with syphilitic interstitial keratitis. *Cornea.* 2001;20:100–103.
10. Elliott GF, Hodson SA. Cornea, and the swelling of polyelectrolyte gels of biological interest. *Rep Prog Phys.* 1998;61:1325–1365.
11. Quantock AJ, Young RD, Akama TO. Structural and biochemical aspects of keratan sulphate in the cornea. *Cell Mol Life Sci.* 2010;67: 891–906.
12. Elliott GF. Measurements of the electric charge and ion-binding of the protein filaments in intact muscle and cornea, with implications for filament assembly. *Biophys J.* 1980;32:95–97.
13. Hodson S, Kaila D, Hammond S, et al. Transient chloride binding as a contributory factor to corneal stromal swelling in the ox. *J Physiol.* 1992;450:89–103.
14. Hodson S, Miller F. The bicarbonate ion pump in the endothelium which regulates the hydration of rabbit cornea. *J Physiol.* 1976;263: 563–577.

- 149 -

Inhibition of TGF-β Signaling Enables Human Corneal Endothelial Cell Expansion *In Vitro* for Use in Regenerative Medicine

Naoki Okumura[1,2], EunDuck P. Kay[1], Makiko Nakahara[1], Junji Hamuro[2], Shigeru Kinoshita[2], Noriko Koizumi[1]*

1 Department of Biomedical Engineering, Faculty of Life and Medical Sciences, Doshisha University, Kyotanabe, Japan, 2 Department of Ophthalmology, Kyoto Prefectural University of Medicine, Kyoto, Japan

Abstract

Corneal endothelial dysfunctions occurring in patients with Fuchs' endothelial corneal dystrophy, pseudoexfoliation syndrome, corneal endotheliitis, and surgically induced corneal endothelial damage cause blindness due to the loss of endothelial function that maintains corneal transparency. Transplantation of cultivated corneal endothelial cells (CECs) has been researched to repair endothelial dysfunction in animal models, though the *in vitro* expansion of human CECs (HCECs) is a pivotal practical issue. In this study we established an optimum condition for the cultivation of HCECs. When exposed to culture conditions, both primate and human CECs showed two distinct phenotypes: contact-inhibited polygonal monolayer and fibroblastic phenotypes. The use of SB431542, a selective inhibitor of the transforming growth factor-beta (TGF-β) receptor, counteracted the fibroblastic phenotypes to the normal contact-inhibited monolayer, and these polygonal cells maintained endothelial physiological functions. Expression of ZO-1 and Na^+/K^+-ATPase maintained their subcellular localization at the plasma membrane. Furthermore, expression of type I collagen and fibronectin was greatly reduced. This present study may prove to be the substantial protocol to provide the efficient *in vitro* expansion of HCECs with an inhibitor to the TGF-β receptor, and may ultimately provide clinicians with a new therapeutic modality in regenerative medicine for the treatment of corneal endothelial dysfunctions.

Introduction

Corneal endothelial dysfunction is a major cause of severe visual impairment leading to blindness due to the loss of endothelial function that maintains corneal transparency. Restoration to clear vision requires either full-thickness corneal transplantation or endothelial keratoplasty. Recently, highly effective surgical techniques to replace corneal endothelium [e.g., Descemet's stripping automated endothelial keratoplasty (DSAEK) and Descemet's membrane endothelial keratoplasty (DMEK)] have been developed [1–3] that are aimed at replacing penetrating keratoplasty for overcoming pathological dysfunctions of corneal endothelial tissue. At present, our group and several other research groups have focused on the establishment of new treatment methods suitable for a practical clinical intervention to repair corneal endothelial dysfunctions [4–9]. Since corneal endothelium is composed of a monolayer and is a structurally flexible cell sheet, corneal endothelial cells (CECs) have been cultured on substrates including collagen sheets, amniotic membrane, or human corneal stroma. Then the cultured CECs are transplanted as a cell sheet. However, these techniques require the use of an artificial or biological substrate that may introduce several problems such as substrate transparency, detachment of the cell sheet from the

cornea, and technical difficulty of transplantation into the anterior chamber. In our effort to overcome those substrate-related problems, we previously demonstrated that the transplantation of cultivated CECs in combination with a Rho kinase (ROCK) inhibitor enhanced the adhesion of injected cells onto the recipient corneal tissue without the use of a substrate and successfully achieved the recovery of corneal transparency in two corneal-endothelial-dysfunction animal models (rabbit and primate) [10,11].

However, in the context of the clinical setting, another pivotal practical issue is the *in vitro* expansion of human CECs (HCECs). HCECs are vulnerable to morphological fibroblastic change under normal culture conditions. Although HCECs can be cultivated into a normal phenotype maintaining the contact-inhibited polygonal monolayer, they eventually undergo massive endothelial-mesenchymal transformation after long-term culture or subculture. Thus, cultivation of HCECs with normal physiological function is difficult, yet not impossible [12,13].

Epithelial mesenchymal transformation (EMT) has been well characterized in epithelial-to-mesenchymal transition, and transforming growth factor-beta (TGF-β) can initiate and maintain EMT in a variety of biological and pathological systems [14,15].
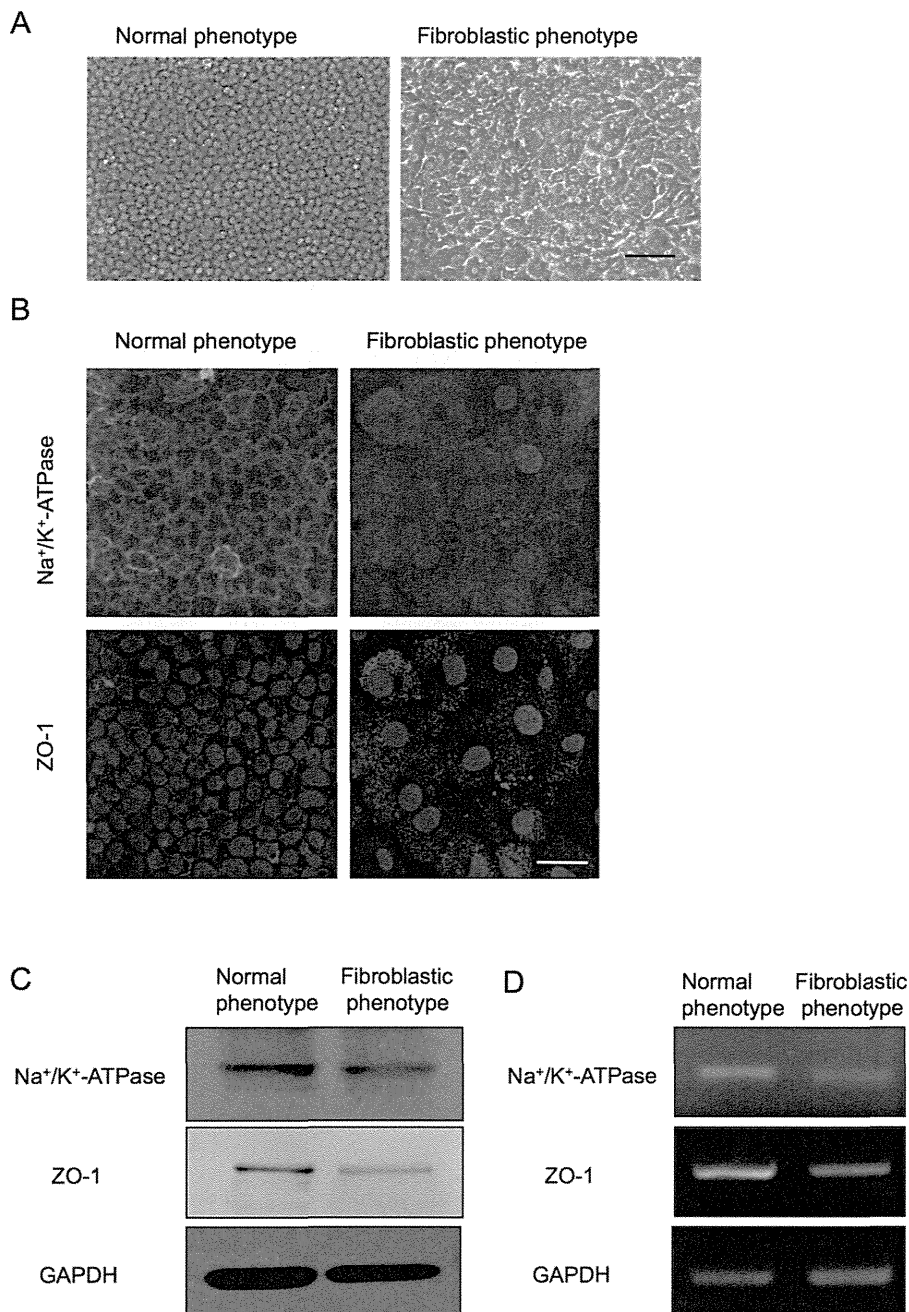
- 150 -

Figure 1. Primate corneal endothelial cells exhibit fibroblastic phenotype and lose functions during cell culture. (A) Cultivated primate CECs demonstrated two distinctive phenotypes; the cells maintained the characteristic polygonal cell morphology and contact-inhibited phenotype (normal phenotype) and the cells showed a fibroblastic cell shape with multi-layering (fibroblastic phenotype). Both phenotypes of the cultured CECs were primary cultured cells. Scale bar: 50 μm. The experiment was performed in triplicate. (B) Na$^+$/K$^+$-ATPase and ZO-1 at the plasma membrane was preserved in the normal phenotype, while fibroblastic phenotype completely lost the characteristic staining profile of Na$^+$/K$^+$-ATPase and ZO-1 at the plasma membrane. Scale bar: 100 μm. (C+D) Expression of the Na$^+$/K$^+$-ATPase and ZO-1 was higher in normal phenotypes than in the fibroblastic phenotypes at both the protein and mRNA levels. Samples were prepared in duplicate. Immunoblotting and semiquantitative PCR were performed in duplicate.
doi:10.1371/journal.pone.0058000.g001

The cellular activity of TGF-β is of particular interest in epithelial cells, as it inhibits the G1/S transition of the cell cycle in these cells. However, the same growth factor is the key signaling molecule for EMT, and the role of TGF-β as a key molecule in the development and progression of EMT is well studied [14–17]. Smad2/3 are signaling molecules downstream of cell-surface receptors for TGF-β in epithelial-to-mesenchymal transition

[16,17]. Similar to epithelial cells, TGF-β inhibits the G1/S transition of the cell cycle in CECs [18,19], however, it is not known how TGF-β develops endothelial to mesenchymal transformation and maintains it in CECs. Endothelial-mesenchymal transformation is observed among corneal endothelial dysfunctions such as Fuchs' endothelial corneal dystrophy, pseudoexfoliation syndrome, corneal endotheliitis, surgically-induced corneal

- 151 -

endothelial damage, and corneal trauma and it induces the fibroblastic transformation of CECs [20–23], suggesting that CECs have the biological potential to acquire endothelial to mesenchymal transformation. The apparent presence of fibroblastic phenotypes in primate CECs and HCECs in culture led us to search for the cause of such phenotypic changes of the cultivated cells and for a means in which to prevent such undesirable cellular changes toward endothelial-mesenchymal transformation.

In the present study, we established primate CEC and HCEC cultures which respectively showed two distinctive phenotypes: 1) normal and 2) fibroblastic. We further characterized the two phenotypes and showed evidence that the use of an inhibitor to TGF-β receptor or BMP-7 abolished the fibroblastic phenotypes of cultivated CECs. Thus, intervention by inhibiting the endothelial to mesenchymal transformation process that occurs during the cultivation of CECs will certainly enable the *in vitro* expansion of cultivated HCECs with a normal phenotype which would be ideal for therapeutic clinical application.

Materials and Methods

Ethics Statement

The monkey tissue used in this study was handled in accordance with the ARVO Statement for the Use of Animals in Ophthalmic and Vision Research. The isolation of the tissue was approved by an institutional animal care and use committee of the Nissei Bilis Co., Ltd. (Otsu, Japan) and the Eve Bioscience, Co., Ltd. (Hashimoto, Japan). The human tissue used in this study was handled in accordance with the tenets set forth in the Declaration of Helsinki. A written consent was acquired from the next of kin of all deceased donors regarding eye donation for research. All tissue is recovered under the tenants of the Uniform Anatomical Gift Act (UAGA) of the particular state where the donor was consented and recovered.

Monkey cornea tissues and Research-grade human cornea tissues

Eight corneas from 4 cynomolgus monkeys (3 to 5 years-of-age; estimated equivalent human age: 5 to 20 years) housed at Nissei Bilis and the Keari Co., Ltd., Osaka, Japan, respectively, were used for the MCECs culture. The cynomolgus monkeys were housed in individual stainless steel cages at Nissei Bilis and Eve Bioscience. Each cage was provided with reverse-osmosis water delivered by an automatic water supply system and supplied with experimental animal diet (PS-A; Oriental Yeast Co., Ltd., Tokyo, Japan). Room temperature was controlled by heating units inside the rooms and was maintained at 18.0–26.0°C. The humidity was maintained at 29.5 to 80.4%. Animals were maintained on a 12:12-h light:dark cycle (lights on, 7 a.m. to 19 p.m.). For other research purposes, the animals were given an overdose of intravenous pentobarbital sodium for euthanatization. The corneas of cynomolgus monkeys were harvested after confirmation of cardiopulmonary arrest by veterinarians, and then provided for our research. Twenty human donor corneas were obtained from the SightLife™ (Seattle, WA) eye bank, and all corneas were stored at 4°C in storage medium (Optisol; Chiron Vision Corporation, Irvine, CA) for less than 14 days prior to the primary culture.

Cell culture of monkey CECs (MCECs)

The MCECs were cultivated in modified protocol as described previously [7,24]. Briefly, the Descemet's membrane including CECs was stripped and digested at 37°C for 2 h with 1 mg/mL collagenase A (Roche Applied Science, Penzberg, Germany). After
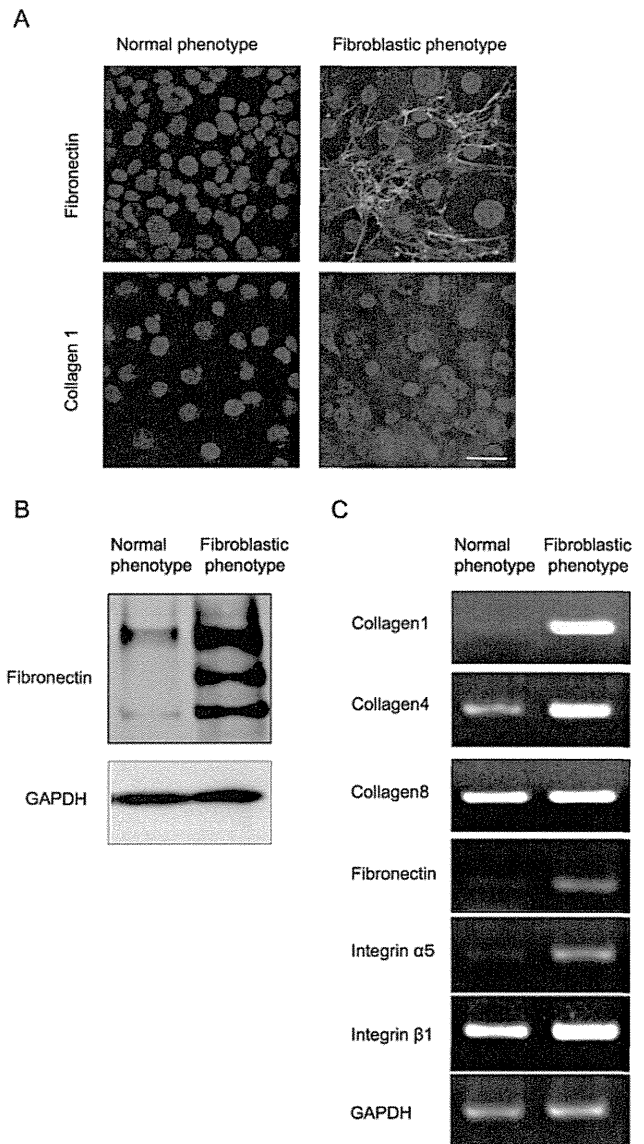

Figure 2. Fibroblastic primate CECs produced an abnormal extra cellular matrix. (A) The fibroblastic phenotype demonstrated excessive ECMs such as fibronectin and collagen type 1, while the normal phenotype completely lost the staining potential. Scale bar: 100 μm. (B) The protein expression level of fibronectin was more strongly upregulated in the fibroblastic phenotype than in the normal phenotype. (C) Semiquantitative PCR analysis showed that the type I collagen transcript [α1(I) mRNA] was abundantly expressed in the fibroblastic phenotypes, while the expression of α1(I) mRNA was reduced in the normal phenotypes. The basement membrane collagen phenotype α1(IV) mRNA was expressed both in normal and fibroblastic phenotypes, yet to a lesser degree in the normal phenotype. Collagen phenotype α1(VIII) mRNA was expressed in both phenotypes at similar levels. Fibronectin and integrin α5 mRNA was observed in the fibroblastic phenotypes, as opposed to the normal phenotypes in which the two transcripts were not expressed. β1 integrin mRNA was expressed in both phenotypes at similar levels. Samples were prepared in duplicate. Immunoblotting and semiquantitative PCR were performed in duplicate.
doi:10.1371/journal.pone.0058000.g002

a digestion at 37°C, the MCECs obtained from individual corneas were resuspended in culture medium and plated in 1 well of a 6-well plate coated with FNC Coating Mix® (Athena Environmental
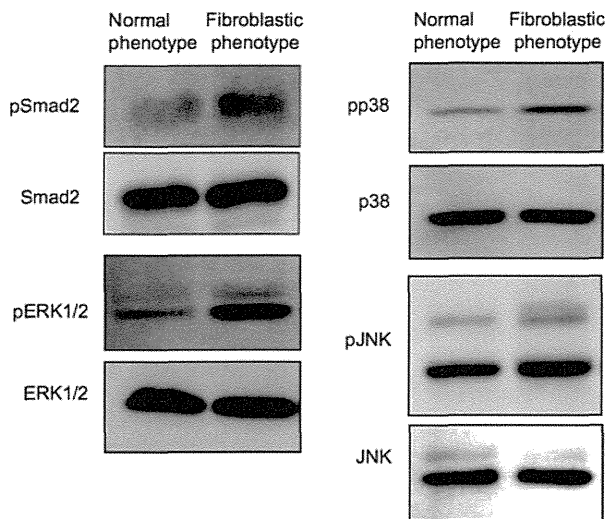
- 152 -

Figure 3. Different activation pattern of fibroblastic change associated pathways in the fibroblastic phenotype of primate CECs. Phosphorylation of Smad2, p38MAPK, and ERK1/2 was promoted in the fibroblastic phenotype compared to that in the normal phenotype, while phosphorylation of JNK was negligible. Samples were prepared in duplicate, and immunoblotting was performed in duplicate.
doi:10.1371/journal.pone.0058000.g003

Sciences, Inc., Baltimore, MD). All primary cell cultures and serial passages of the MCECs were performed in growth medium composed of Dulbecco's modified Eagle's medium (Invitrogen Corporation, Carlsbad, CA) supplemented with 10% fetal bovine serum (FBS), 50 U/mL penicillin, 50 µg/mL streptomycin, and 2 ng/mL FGF-2 (Invitrogen). The MCECs were then cultured in a humidified atmosphere at 37°C in 5% CO_2, and the culture medium was changed every 2 days. When the MCECs reached confluency in 10 to 14 days, they were rinsed in Ca^{2+} and Mg^{2+}-free Dulbecco's phosphate-buffered saline (PBS), trypsinized with 0.05% Trypsin-EDTA (Invitrogen) for 5 min at 37°C, and passaged at ratios of 1:2–4. Cultivated MCECs at passages 2 through 5 were used for all experiments. SB431542 (Merck Millipore, Billerica, MA), a selective inhibitor of transforming growth factor-β (TGF-beta), was tested for the anti-fibroblastic effect.

Cell culture of HCECs

The HCECs were cultivated in a modified version of the protocol used for the MCECs. Briefly, the Descemet's membrane including CECs was stripped and digested at 37°C for 2 h with 1 mg/mL collagenase A (Roche Applied Science). After a digestion at 37°C, the HCECs obtained from individual corneas were resuspended in culture medium and plated in 1 well of a 12-well plate coated with FNC Coating Mix®. The culture medium was prepared according to published protocols [25], but with some modifications. Briefly, basal culture medium containing Opti-MEM-I (Invitrogen), 8% FBS, 5 ng/mL epidermal growth factor (EGF) (Sigma-Aldrich Co., St. Louis, MO), 20 µg/mL ascorbic acid (Sigma-Aldrich), 200 mg/L calcium chloride (Sigma-Aldrich), 0.08% chondroitin sulfate (Wako Pure Chemical Industries, Ltd., Osaka, Japan), and 50 µg/mL of gentamicin was prepared, and the conditioned medium was then recovered after cultivation of inactivated 3T3 fibroblasts. Inactivation of the 3T3 fibroblasts was performed as described previously [26,27]. Briefly, confluent 3T3 fibroblasts were incubated with 4 µg/mL mitomycin C (MMC)

(Kyowa Hakkko Kirin Co., Ltd., Tokyo, Japan) for 2 h at 37°C under 5% CO_2, and then trypsinized and plated onto plastic dishes at the density of 2×10^4 cells/cm^2. The HCECs were cultured in a humidified atmosphere at 37°C in 5% CO_2, and the culture medium was changed every 2 days. When the HCECs reached confluency in 14 to 28 days, they were rinsed in Ca^{2+} and Mg^{2+}-free PBS, trypsinized with 0.05% Trypsin-EDTA for 5 min at 37°C, and passaged at ratios of 1:2. Cultivated HCECs at passages 2 through 5 were used for all experiments. To test the anti-fibroblastic effect, the cultured HCECs were passaged at the ratio of 1:2 with medium supplemented with or without SB431542 (0.1, 1, and 10 µM) (Merck Millipore), a neutralizing antibody to TGF-β (500 ng/ml) (R&D Systems, Inc., Minneapolis, MN), Smad3 inhibitor (3 mM) (Merck Millipore), and bone morphogenetic protein (BMP) BMP-7 (10, 100, and 1000 ng/ml) (R&D Systems), and were then evaluated after 1 week.

Histological examination

For histological examination, cultured MCECs or HCECs on Lab-Tek™ Chamber Slides™ (NUNC A/S, Roskilde, Denmark) were fixed in 4% formaldehyde for 10 min at room temperature (RT) and incubated for 30 min with 1% bovine serum albumin (BSA). To investigate the phenotype of the CECs, immunohistochemical analyses of ZO-1 (Zymed Laboratories, Inc., South San Francisco, CA), a tight junction associated protein, Na^+/K^+-ATPase (Upstate Biotechnology, Inc., Lake Placid, NY), the protein associated with pump function, fibronectin (BD, Franklin Lakes, NJ), and actin were performed. ZO-1 and Na^+/K^+-ATPase were used as function related markers of the CECs, fibronectin and collagen type 1 were used to evaluate the fibroblastic change, and actin staining was used to evaluate the cellular morphology. The ZO-1, Na^+/K^+-ATPase, collagen type 1, and fibronectin staining were performed with a 1:200 dilution of ZO-1 polyclonal antibody, Na^+/K^+-ATPase monoclonal antibody, and fibronectin monoclonal antibody, respectively. For the secondary antibody, a 1:2000 dilution of Alexa Fluor® 488-conjugated or Alexa Fluor® 594-conjugated goat anti-mouse IgG (Invitrogen) was used. Actin staining was performed with a 1:400 dilution of Alexa Fluor® 488-conjugated phalloidin (Invitrogen). Cell nuclei were then stained with DAPI (Vector Laboratories, Inc., Burlingame, CA) or propidium iodide (PI) (Sigma-Aldrich). The slides were then inspected by fluorescence microscopy (TCS SP2 AOBS; Leica Microsystems, Wetzlar, Germany). The percentages of Na^+/K^+-ATPase- and ZO-1-positive cells that expressed Na^+/K^+-ATPase and ZO-1 at the plasma membrane in the *in vivo* condition were counted by a blinded examiner.

Immunoblotting

For immunoblotting, the cells were washed with PBS and then lysed with radio immunoprecipitation assay (RIPA) buffer (Bio-Rad Laboratories, Hercules, CA) containing Phosphatase Inhibitor Cocktail 2 (Sigma-Aldrich) and Protease Inhibitor Cocktail (Nacalai Tesque, Kyoto, Japan). The lysates were then centrifuged at 15,000 rpm for 10 min at 4°C. The resultant supernatant was collected and the protein concentration of the sample was assessed with the BCA™ Protein Assay Kit (Takara Bio Inc., Otsu, Japan). The proteins were then separated by sodium dodecyl sulfate polyacrylamide gel electrophoresis (SDS-PAGE) and transferred to polyvinylidene fluoride (PVDF) membranes. The membranes were then blocked with 3% non-fat dry milk (Cell Signaling Technology, Inc., Danvers, MA) in TBS-T buffer. The incubations were then performed with the following primary antibodies: Na^+/K^+-ATPase (Merck Millipore), ZO-1, GAPDH (Abcam, Cambridge, UK), fibronectin, and Smad2 (Cell Signaling Technology),
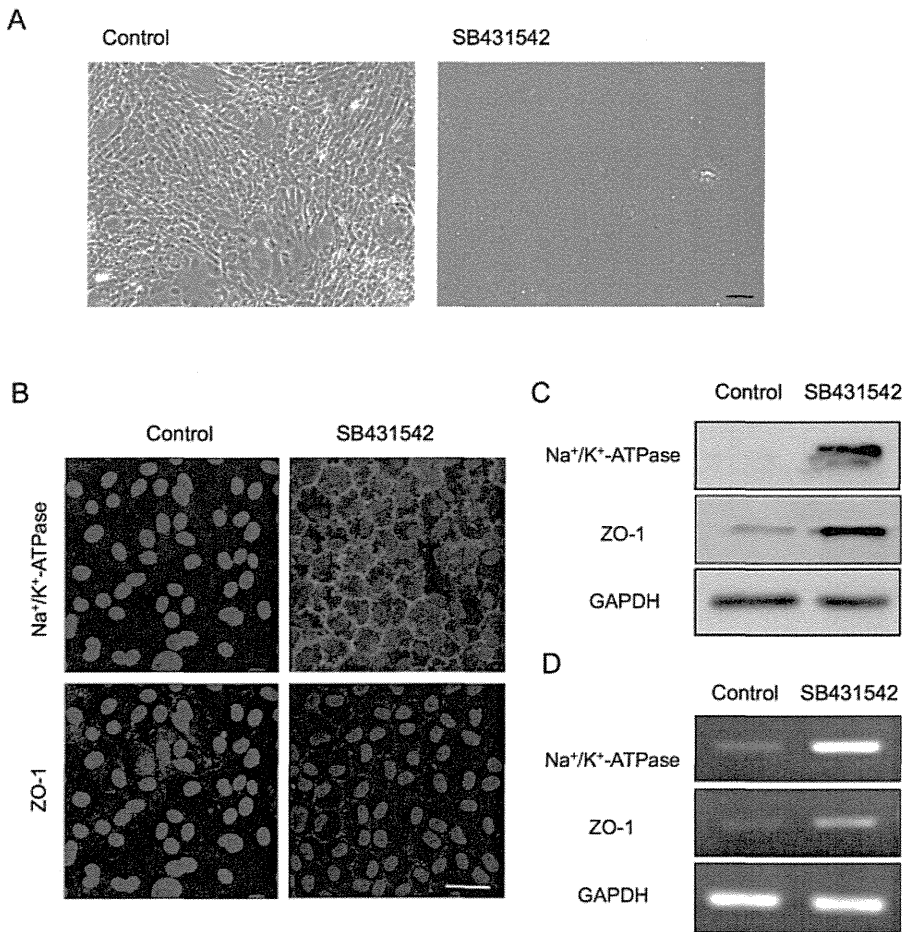
- 153 -

Figure 4. Inhibition of the TGF-β pathway suppressed fibroblastic change and maintained functions. (A) Primate CECs cultured with SB431542 exhibited the authentic polygonal cell shape and contact-inhibited monolayer, while the control CECs exhibited the fibroblastic morphology. Scale bar: 50 μm. (B) SB431542-treated CECs showed the characteristic plasma membrane staining of Na$^+$/K$^+$-ATPase and ZO-1, while the control CECs lost their staining. Scale bar: 100 μm. (C+D) Expression of Na$^+$/K$^+$-ATPase and ZO-1 was greatly upregulated in the SB431542-treated fibroblastic phenotypes at both the protein and mRNA levels. Samples were prepared in duplicate. Immunoblotting and semiquantitative PCR were performed in duplicate.
doi:10.1371/journal.pone.0058000.g004

phosphorylated Smad2 (Cell Signaling Technology), ERK1/2 (BD), phosphorylated ERK1/2 (BD), p38MAPK (BD), phosphorylated p38MAPK (BD) JNK (BD) or phosphorylated JNK (BD) (1:1000 dilution), and HRP-conjugated anti-rabbit or anti-rabbit IgG secondary antibody (Cell Signaling Technology) (1:5000 dilution). Membranes were exposed by ECL Advance Western Blotting Detection Kit (GE Healthcare, Piscataway, NJ), and then examined by use of the LAS4000S (Fujifilm, Tokyo, Japan) imaging system.

Semiquantitative reverse transcriptase polymerase chain reaction (RT-PCR) and quantitative PCR

Total RNA was extracted from CECs and cDNA was synthesized by use of ReverTra Ace® (Toyobo, Osaka, Japan), a highly efficient RT. The same amount of cDNA was amplified by PCR (GeneAmp 9700; Applied Biosystems) and the following primer pairs: GAPDH mRNA, forward (5′-GAGTCAACG-GATTTGGTCGT-3′), and reverse (5′-TTGATTTTGGAGG-GATCTCG-3′); Na$^+$/K$^+$-ATPase mRNA, forward (5′-CTTCCTCCGCATTTATGCTCATTTTCTCACCC-3′), and reverse (5′-GGATGATCATAAACTTAGCCTTGAT-GAACTC-3′); ZO-1 mRNA, forward (5′-GGACGAGGCAT-

CATCCCTAA-3′), and reverse (5′-CCAGCTTCTCGAA-GAACCAC-3′); collagen1 mRNA, forward (5′-TCGGCGAGAGCATGACCGATGGAT-3′), and reverse (5′-GACGCTGTAGGT GAAGCGGCTGTT-3′); collagen4 mRNA, forward (5′-AGCAAGGTGTTACAGGATTGGT -3′), and reverse (5′- AGAAGGACACTGTGGGTCATCT -3′); collagen8 mRNA, forward (5′-ATGT-GATGGCTGTGCTGCTGCTGCCT -3′), and reverse (5′-CTCTTGGGCCAGGCTCTCCA-3′); fibronectin mRNA, forward (5′-AGATGAGTGGGAACGAATGTCT -3′), and reverse (5′-GAGGGTCACACTTGAATTCTCC -3′); integrin α5 mRNA, forward (5′-TCCTCAGCAAGAATCTCAACAA -3′), and reverse (5′-GTTGAGTCCCGTAACTCTGGTC -3′); integrin β1 mRNA, forward (5′-GCTGAAGACTATCCCATT-GACC -3′), and reverse (5′-ATTTCCAGA-TATGCGCTGTTTT -3′). PCR products were analyzed by agarose gel electrophoresis. Quantitative PCR was performed using the following TaqMan® (Invitrogen) primers: collegen1, Hs00164004_m1; fibronectin, Hs01549976_m1; GAPDH, Hs00266705_g1. The PCR was performed using the StepOne™ (Applied Biosystems) real-time PCR system. GAPDH was used as an internal standard.
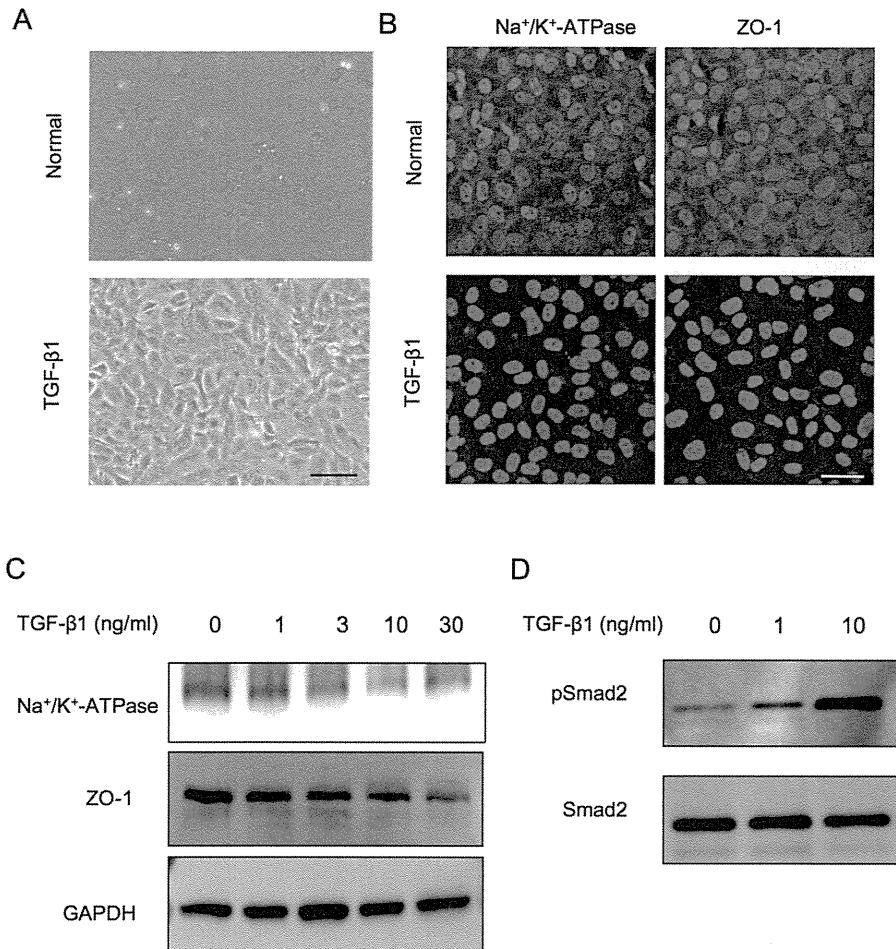
- 154 -

Figure 5. TGFβ induced fibroblastic change and function loss through the activation of the Smad signaling pathways. (A) Normal phenotype primate CECs were transformed to fibroblastic cells when exposed to the exogenous TGF-β1 (10 ng/ml). Scale bar: 50 μm. (B) The staining pattern of Na$^+$/K$^+$-ATPase and ZO-1 at the plasma membrane of the normal phenotypes was greatly reduced upon exposure to TGF-β1 (10 ng/ml). Scale bar: 100 μm. (C) TGF-β1 reduced the expression of Na$^+$/K$^+$-ATPase and ZO-1 at protein levels dose-dependently. (D) Phosphorylation of Smad2 was increased in a concentration-dependent manner. Samples were prepared in duplicate, and immunoblotting was performed in duplicate. doi:10.1371/journal.pone.0058000.g005

Enzyme-linked immunosorbent assay (ELISA)

Collagen type I of culture medium supernatant of HCECs were measured using ELISA kits for Collagen Type I Alpha 2 (COL1a2) (Uscn Life Science Inc., Wuhan, China) according to the manufacturer's instructions. Culture medium supernatant from HCECs cultured with or without SB431542 were used for each group (n = 5).

Statistical analysis

The statistical significance (*P*-value) in mean values of the two-sample comparison was determined by use of the Student's t-test. The statistical significance in the comparison of multiple sample sets was analyzed by use of the Dunnett's multiple-comparisons test. Values shown on the graphs represent the mean ± SE.

Results

Two distinct phenotypes of primate CECs during cell culture

Of great interest, the primate CECs in culture demonstrated two distinctive phenotypes when determined by cell morphology and the characteristic contact-inhibited phenotype. Although to culture primate CECs in a normal phenotype while maintaining the monolayer contact-inhibited morphology is possible, they often showed morphological fibroblastic change after primary culture following isolation from the cornea, or long-term culture or subculture, if they were once primary cultured in normal morphology (Fig. 1A). The two phenotypes were then tested for the endothelial characteristics; the staining pattern of Na$^+$/K$^+$-ATPase and ZO-1 at the plasma membrane was well preserved in the normal phenotypes, yet the fibroblastic phenotypes completely lost the characteristic staining profile of Na$^+$/K$^+$-ATPase and ZO-1 at the plasma membrane (Fig. 1B). Expression of the two functional proteins was found to be much greater in the normal phenotypes than in the fibroblastic phenotypes at both the protein (Fig. 1C) and mRNA levels (Fig. 1D). Comparison of the expression of authentic fibrillar extracellular matrix (ECM) proteins showed that fibroblastic phenotypes demonstrated a fibrillar ECM staining pattern of fibronectin, while the normal phenotypes completely lost the staining potential of fibronectin (Fig. 2A). The protein expression level of fibronectin was more strongly upregulated in the fibroblastic phenotypes than in the normal phenotypes (Fig. 2B). Type I collagen produced by fibroblastic phenotypes demonstrated dual locations, at the ECM
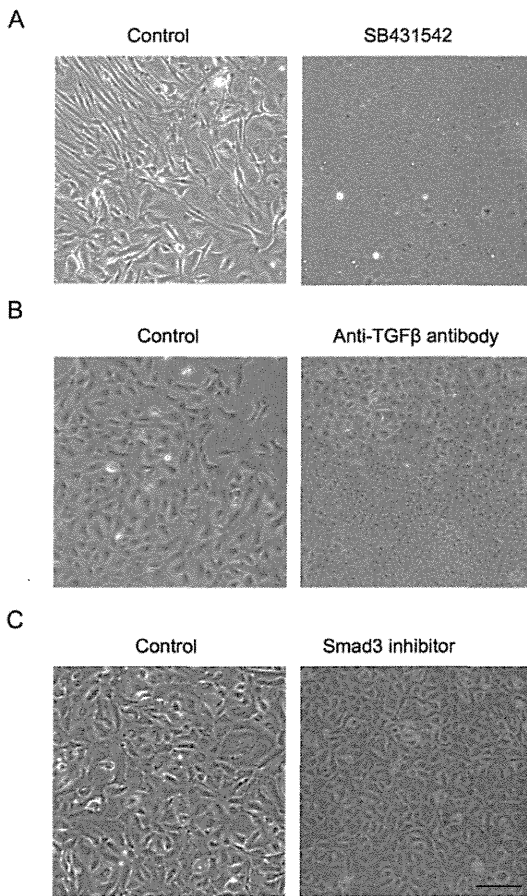
- 155 -

A

Control   SB431542

B

Control   Anti-TGFβ antibody

C

Control   Smad3 inhibitor

Figure 6. Inhibition of the TGFβ pathway suppressed the fibroblastic change of HCECs. (A) HCECs cultured with SB431542 (1 μM) exhibited the hexagonal cell shape and contact-inhibited monolayer, while the control CECs exhibited the fibroblastic morphology. (B+C) Both neutralizing antibody to TGF-β (500 ng/ml) and Smad3 inhibitor (3 mM) blocked cells from acquiring fibroblastic phenotypes. Scale bar: 50 μm. The experiment was performed in duplicate.
doi:10.1371/journal.pone.0058000.g006

the MAPKs were involved in an endothelial-mesenchymal transformation similar to the EMT observed in epithelial cells (Fig. 3). Phosphorylation of Smad2 was found to be greatly promoted in the fibroblastic phenotypes when compared to that in the normal phenotypes. Phosphorylation of p38 and ERK1/2 was greatly enhanced in the fibroblastic phenotypes, while activation of JNK was negligible. These findings suggested that TGF-β signaling may exert the key role for the fibroblastic transformation of CECs.

TGF-β-mediated endothelial-mesenchymal transformation and use of TGF-β receptor inhibitor to block it in primate CECs

The findings shown in Fig. 3 led us to directly test whether SB431542, the TGF-β receptor inhibitor, was able to block the EMT process observed in the fibroblastic phenotypes. Phase contrast imaging demonstrated that primate CECs cultured in the presence of SB431542 exhibited the authentic polygonal cell shape and contact-inhibited monolayer, while the control CECs exhibited the fibroblastic morphology (Fig. 4A). Moreover, the SB431542-treated CECs showed the characteristic plasma membrane staining of Na$^+$/K$^+$-ATPase and ZO-1, while the control CECs lost their staining, suggesting that endothelial functions were maintained in the SB431542-treated cells (Fig. 4B). Furthermore, the expression of Na$^+$/K$^+$-ATPase and ZO-1 was strongly upregulated in the SB431542-treated fibroblastic phenotypes at both the protein (Fig. 4C) and mRNA levels (Fig. 4D). These data further confirmed that TGF-β might be the direct mediator of the endothelial to mesenchymal transformation observed in primate CEC cultures. Therefore, we tested whether the normal phenotypes were transformed to fibroblastic cells when exposed to the exogenous TGF-β, as in the findings shown in Fig. 5A. Of interest, the staining pattern of Na$^+$/K$^+$-ATPase and ZO-1 at the plasma membrane of the normal phenotypes was greatly reduced upon exposure of polygonal cells to TGF-β (Fig. 5B). The growth factor also markedly reduced the expression of the two proteins at protein levels in a concentration-dependent manner (Fig. 5C), while phosphorylation of Smad2 was greatly increased in a concentration-dependent manner (Fig. 5D). These data suggest that even the normal phenotypes of primate CECs are prone to acquire fibroblastic phenotypes in response to TGF-β-stimulation.

Two distinct phenotypes of HCEC cultures and the use of TGF-β receptor inhibitor to block endothelial-mesenchymal transformation

The interesting findings observed in primate CECs led us to further study whether HCECs were subjected to the similar undesirable prerequisite cellular changes leading to endothelial-mesenchymal transformation. Of great interest, cultivated HCECs lost the characteristic contact-inhibited monolayer and polygonal phenotypes, and acquired fibroblastic cell morphology like primate CECs (Fig. 6A). However, consistent with the primate CECs when the CECs were cultivated with the specific inhibitor to the TGF-β receptor (SB431542), the inhibitor was able to block alteration of the cell shape to fibroblastic phenotypes. Similar to the inhibitory effect of SB431542 on fibroblastic phenotypes, both neutralizing antibody to TGF-β (Fig. 6B) and Smad3 inhibitor (Fig. 6C) also blocked cells from acquiring fibroblastic phenotypes. We then tested whether SB431542 was able to maintain endothelial function. The findings shown in Fig. 7A and Fig. 7B demonstrated that blocking the TGF-β receptor signaling enabled the subcellular localization of Na$^+$/K$^+$-ATPase and ZO-1 at the plasma membrane and their protein expression to be maintained. Of

and at the cytoplasm. Of interest, the cytoplasmic location of type I collagen appeared to be at the Golgi complex, the intracellular localization of which is essential for secretion, and these findings are similar to the published data [28]. On the other hand, type I collagen staining in the normal phenotypes was not clearly observed (Fig. 2A). RT-PCR analysis was used to determine the expression of major ECM proteins. The type I collagen transcript [α1(I) mRNA] was found to be abundantly expressed in the fibroblastic phenotypes, while the expression of α1(I) mRNA was negligible in the normal phenotypes (Fig. 2C). Unlike the type I collagen transcript, the basement membrane collagen phenotype α1(IV) mRNA was expressed in both the normal and fibroblastic phenotypes, yet to a lesser degree in the normal phenotype. Collagen phenotype α1(VIII) mRNA was expressed in both phenotypes at similar levels. Expression of fibronectin and integrin α5 was observed in the fibroblastic phenotypes, as opposed to the normal phenotypes in which the two transcripts were not expressed (Fig. 2C). On the other hand, β1 integrin mRNA was expressed in both phenotypes at similar levels (Fig. 2C).

Next, signaling pathways were determined to elucidate what might cause fibroblastic phenotypes of CECs. Since Smad2, p38, ERK1/2, and JNK are reportedly all involved in the EMT pathway [18–20,29,30], we therefore tested whether Smad2 and
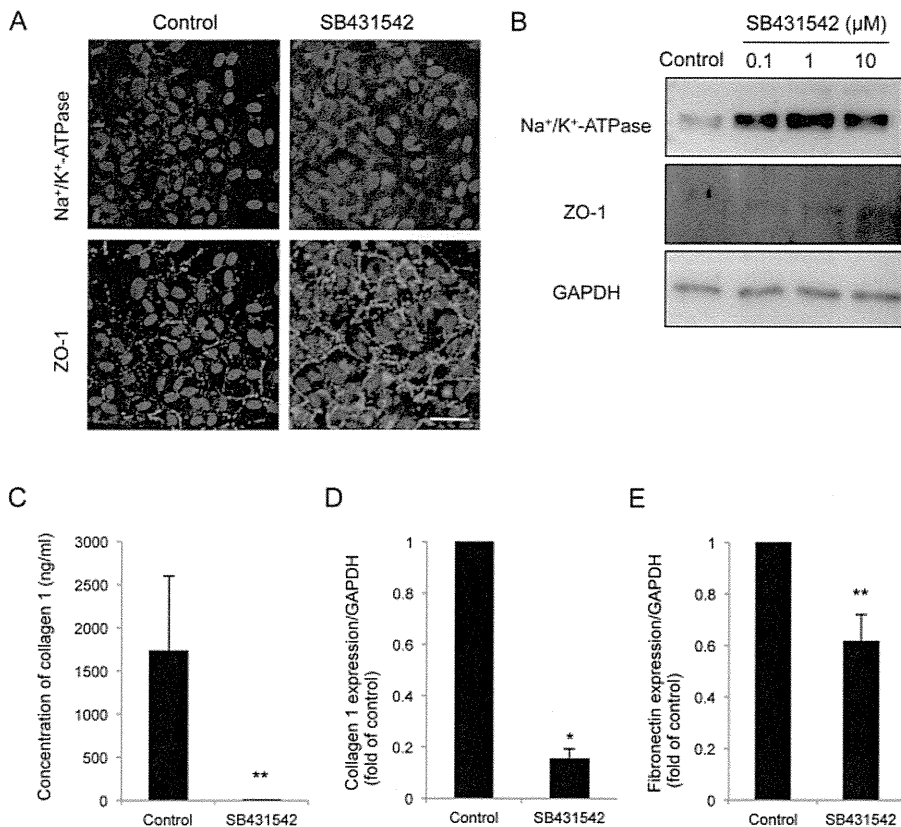
- 156 -

Figure 7. SB431542 maintained the functions and suppressed the fibroblastic change of HCECs. (A+B) Blocking the TGF-receptor signaling by SB431542 (A: 1 μM, B: 0.1, 1, and 10 μM) enabled the subcellular localization of Na$^+$/K$^+$-ATPase and ZO-1 at the plasma membrane and their protein expression to be maintained. Scale bar: 100 μm. (C) ELISA assay revealed that SB431542 significantly downregulated the secretion of type I collagen to the culture supernatant. **P<0.05. (D+E) Quantitative PCR showed that SB431542 significantly reduced the expression of type I collagen and fibronectin at the mRNA level. *p<0.01, ** p<0.05. Samples were prepared in duplicate. Immunoblotting, ELISA, and quantitative PCR were performed in duplicate.
doi:10.1371/journal.pone.0058000.g007

great importance, ELISA assay revealed that SB431542 markedly downregulated the secretion of type I collagen to the culture supernatant (Fig. 7C). Coincidentally, SB431542 markedly reduced the expression of type I collagen and fibronectin at the mRNA level (Fig. 7D, E).

Use of BMP-7 to suppress fibroblastic changes and maintain endothelial functions

Bone morphogenetic protein-7 (BMP-7) promotes MET and specifically inhibits the TGF-β-mediated epithelial-to-mesenchymal transition. Thus, that molecule has been used to antagonize the EMT process [31–34]. We therefore tested whether BMP-7 was able to antagonize the prerequisite changes of HCECs. The fibroblastic HCECs were treated with BMP-7 in a concentration ranging from 10 to 1000 ng/ml. Of important note, the elongated cell shapes of the fibroblastic phenotypes were reversed to the polygonal cell morphology in response to the presence of BMP-7 in a concentration-dependent manner (Fig. 8A). BMP-7 enabled the hexagonal cell morphology and actin cytoskeleton distribution at the cortex to be maintained (Fig. 8B), similar to that observed in normal CECs [35], and it also maintained the subcellular localization of Na$^+$/K$^+$-ATPase (Fig. 8C) and ZO-1 (Fig. 8D) at the plasma membrane. Thus, BMP-7 at the concentration of 1000 ng/ml was able to maintain CECs in polygonal and contact-inhibited phenotypes with a positive expression of function-related markers (Fig. 8E, F).

Discussion

Corneal endothelial dysfunction accompanied by visual disturbance is a major indication for corneal transplantation surgery [36,37]. Though corneal transplantation is widely performed for corneal endothelial dysfunction, researchers are currently seeking alternative methods to restore healthy corneal endothelium. The fact that corneal endothelium is cultured and stocked as 'master cells' from young donors allows for the transplantation of CECs with high functional ability and for an extended period of time. In addition, an HLA-matching transplantation to reduce the risk of rejection [38,39] and overcoming the shortage of donor corneas might be possible. Tissue bioengineering is a new approach to develop treatments for patients who have lost visual acuity [40]. To date, there are two methods that utilize bioengineering approaches: 1) use of cultured donor HCECs adhered on bioengineered constructs [4,5,7,9], and 2) transplantation of cultivated HCECs into the anterior chamber [11,41–43]. Regardless of which of the two methods is applied to clinical settings, establishment of an efficient cultivation technique for HCECs is essential and inevitable [44]. Many researchers have noticed that establishing a consistent long-term culture of HCECs is challenging [40]. Although the successful cultivation of HCECs has been reported by several groups, the procedures involved in the isolation and subsequent cultivation protocols varied greatly between laboratories [44]. One of the most difficult problems is

- 157 -